Sialylation of Asparagine 612 inhibits Aconitase activity during mouse sperm capacitation; A possible mechanism for the switch from oxidative phosphorylation to glycolysis.

Ana Izabel Silva Balbin Villaverde[1], Rachel Ogle[1], Peter Lewis[2], Louise Hetherington[1], Vince Carbone[3] Tony Velkov[4], Jacob Netherton[1], Mark A. Baker[1]

[1] Priority Research Centre in Reproductive Science, School of Environmental and Life Sciences, University of Newcastle, Callaghan, NSW, Australia

[2] Centre for Chemical Biology and Clinical Pharmacology, Department of Biology, School of Environmental & Life Sciences, The University of Newcastle, Callaghan

[3]AgResearch, Grasslands Research Centre, Tennent Drive, Private Bag 11008, Palmerston North 4442, New Zealand.

[4] Faculty of Pharmacy and Pharmaceutical Sciences, Monash University, NSW, Australia

This work was supported by the Brazilian National Council for Scientific and Technological Development (CNPq).

Correspondence: Mark A. Baker, Priority Research Centre in Reproductive Science, School of Environmental and Life Sciences, University of Newcastle, Callaghan, NSW 2308, Australia.
Tel: +61 2 4921 6143: Fax: +61 2 4921 6308 E-mail: Mark.Baker@newcastle.edu.au

Abstract

After ejaculation, mammalian spermatozoa must undergo a process known as capacitation in order to successfully fertilize the oocyte. Several post-translational modifications occur during capacitation, including sialylation, which despite being limited to a few proteins, seems to be essential for proper sperm-oocyte interaction. Regardless of its importance, to date, no single study has ever identified nor quantified which glycoproteins bearing terminal sialic acid (Sia) are altered during capacitation. Here we characterize sialylation during mouse sperm capacitation. Using tandem mass spectrometry coupled with liquid chromatography (LC-MS/MS), we found 142 non-reductant peptides, with 9 of them showing potential modifications on their sialylated oligosaccharides during capacitation. As such, N-linked sialoglycopeptides from C4b-binding protein, endothelial lipase (EL), serine proteases 39 and 52, testis-expressed protein 101 and zonadhesin were reduced following capacitation. In contrast, mitochondrial aconitate hydratase (aconitase; ACO2) was the only protein to show an increase in Sia content during capacitation. Interestingly, while the loss of Sia within EL (N62) was accompanied by a reduction in its phospholipase A_1 activity, the increase of sialylation in the ACO2 (N612) also resulted in a decrease of the activity of this TCA cycle enzyme. The latter was confirmed by N612D recombinant protein with both His and GFP tag, in which the N612D mutant had no activity compared to WT when protein. Computer modelling show that N612 sits atop the catalytic site of ACO2. The introduction of sialic acid causes a large confirmation change in the alpha helix, essentially, distorting the active site, leading to complete loss of function. These findings suggest that the switch from oxidative phosphorylation, over to glycolysis that occurs during capacitation may come about through sialylation of ACO2.

Keywords: glycoproteins, sialic acid, titanium dioxide, LC-MS/MS, endothelial lipase.

Abbreviations: acetonitrile (ACN), asparagine (Asn), dibutyryl-cAMP (dbcAMP), endothelial lipase (EL), liquid chromatography tandem-mass spectrometry (LC-MS/MS), mass spectrometry (MS), meprin/A5 antigen/mu receptor tyrosine phosphatase (MAM), mitochondrial aconitate hydratase (ACO2), peptide-N-glycosidase F (PNGase F), phospholipase A_1 (PLA_1), phospholipase A_1 selective substrate (PED-A_1), serine (Ser), sialic acid (Sia), threonine (T), Aspartic acid (D), titanium dioxide (TiO_2), tricarboxylic acid (TCA), trifluoroacetic acid (TFA), wild-type ACO2 transfected (WT).

Introduction

Sperm capacitation is a phenomenon first described by Chang, who demonstrated that freshly ejaculated spermatozoa are unable to fertilize the oocyte immediately [1]. Rather, a period within the female reproductive tract was required [1]. During this period, it is evident that spermatozoa undergo a series of biochemical and metabolic changes to become fully capable of fertilizing the egg [2-4]. From a metabolic perspective, Fraser and Lane first described the phenomenon of a metabolic switch that occurs during capacitation [5]. In this context, freshly ejaculated spermatozoa have high rates of oxygen consumption, however, during *in vitro* capacitation, mouse spermatozoa decrease their reliance on oxidative phosphorylation and switch over to a glycolytic pathway [5]. Using different metabolic substrates, this "switch" was shown to be necessary to achieve fertilization [5]. In addition, the reliance on glycolysis explain why sperm-specific glycolytic knockout mice, including GADPH [6], are infertile due to poor motility. From a biochemical perspective, it is unknown how sperm make this switch. However, considering that

spermatozoa are transcriptionally and translationally silent, with the exception of mitochondrial proteins [7], we reasoned that post-translational modifications of existing proteins would likely play a role [8].

Whilst the role of phosphorylation in sperm capacitation is well studied [9-11], few studies have looked at the specific role of protein glycosylation. The latter is characterized by the addition of oligosaccharide side chains via a covalent linkage either at the asparagine (Asn) residue (N-linked) or at the serine/threonine (Ser/Thr) residues (O-linked). There are a number of variations in terms of glycan structures, which is translated in a wide range of biological functions [12, 13]. Notably, terminal sugar sequences are among the features suggested as mediators of more specific roles [12]. In this context, sialic acid (Sia), a monosaccharide with a nine-carbon backbone and negatively charged, is considered an important terminal sugar.

The presence of Sia residues in glycoconjugates at the sperm surface seems to be vital for the success of fertilization. Indeed, in both humans [14] and boars [15] with unexplained infertility or subfertility, a decreased affinity for the lectin wheat germ agglutinin (WGA) has been reported, suggesting either N-acetyl glucosamine and Sia residues are lacking within these cells. Interestingly, surface Sia residues have also been shown to help sperm to survive and migrate inside the female reproductive tract by reducing their phagocytosis and antigenicity [16-18] and by helping them to penetrate the cervical mucus [19]. During sperm capacitation, it has been suggested that Sia residues are shed from the surface of spermatozoa. In this context, studies using lectin binding [20-23], surface charge determination [24, 25] radiolabeling of terminal sialyl residues [26] and HPLC measurement following acid hydrolysis [27] have all indicated that surface sialoglycoconjugates are probably lost or modified when spermatozoa are incubated under capacitating conditions. One model that has been put forward is that the shedding of Sia residues

may be triggered by the release of neuraminidases present at the sperm surface [27]. If this is the case, then the presence of oviduct fluid components [21] heparin [22] and/or albumin [28] in the medium probably facilitate this release [27].

Despite the data that show changes in sperm sialylation content during capacitation, no single publication has ever look at which proteins are sialylated in spermatozoa, yet alone quantified their levels during capacitation. With this in mind, we used titanium dioxide (TiO_2) followed by peptide-N-glycosidase F (PNGase F) cleavage to search for N-linked Sia-containing peptides and to quantify them during *in vitro* capacitation of mouse sperm. In addition, we further studied both mitochondrial aconitate hydratase (aconitase; ACO2) and endothelial lipase (EL) proteins to demonstrate a biologically meaningful effect of the Sia residue during sperm capacitation.

Material and Methods

Materials

Chemicals were purchased from Sigma-Aldrich at highest research grade with the exception of the following products. Chloroform was purchased from Fronine (Riverstone, NSW, Australia). The 2-D quant kit was from G.E. Healthcare (Castle Hill, NSW, Australia). BCA assay kit was from Quantum Scientific (Pierce, Milton, QLD, Australia). HEPES was from Invitrogen Australia (Melbourne, VIC, Australia). Sequencing grade trypsin was supplied by Promega (Alexandria, NSW, Australia). Antarctic phosphatase and PNGase F were purchased from New England Biolabs (Arundel, QLD, Australia). Phospholipase A_1 selective substrate (PED-A_1) (N-((6-(2,4-DNP)Amino)Hexanoyl)-1-(BODIPY® FL C5)-2-Hexyl-Sn-Glycero-3-Phosphoethanolamine) was purchased from Molecular Probes (Melbourne, VIC, Australia). The TiO_2 was collected from

a disassembled column. Ionophore A23187 was purchased from Calbiochem (EMD Biosciences, La Jolla, USA).

Sperm collection and in vitro capacitation

Animal use was approved by institutional and New South Wales State Government ethics committees. Adult Swiss mice (~8-10 weeks) were euthanized and the epididymides were removed. Sperm cells were recovered from the cauda of the epididymides using retrograde flushing [29, 30] and then incubated for 10 min at 37ºC in 0.3% BSA BWW media to allow cell dispersion [31]. For the non-capacitated group, sodium bicarbonate was replaced by sodium chloride in the BWW media. Pentoxifylline and dibutyryl-cAMP (dbcAMP) were added only in the capacitated group at a final concentration of 1mM each. All samples were incubated for 60 min at 37ºC and then sperm cells were washed three times (300 x g, 3 min) using BWW media without BSA.

Protein extraction and sialoglycopeptide enrichment

Sperm pellets were resuspended in a lysis buffer consisting of 1% (w/v) C7BzO [3-(4-Heptyl) phenyl-3-hydroxypropyl) dimethylammoniopropanesulfonate], 7 M urea, 2 M thiourea, and 40 mM Tris (pH 10.4) at a final concentration of ~2.5 x 10^6/ 100 µL and incubated for 1 h (4°C) with constant rotation. Supernatant (18,000 x g, 15 min, 4°C) was recovered and total protein was quantified using a 2-D quant kit following manufacture's protocol. Proteins were reduced (10 mM DTT, 30 min, 30ºC), alkylated (45 mM iodoacetamide, 30 min, 30ºC) and 250 µg of protein was

131 precipitated using methanol and chloroform [32]. Samples were incubated overnight (37ºC) with
132 trypsin at a 1:50 (trypsin/protein) ratio. Proteases were inactivated (bath sonication, 15 minutes)
133 and peptides were treated with alkaline phosphatase (20 U, 2 hours, 30ºC).

134 Enrichment of glycopeptides containing terminal Sia was performed as previously described [33].
135 In brief, peptide samples were diluted in loading buffer [1 M glycolic acid, 80% (v/v) ACN, 5%
136 (v/v) TFA] and then applied to TiO_2 beads (2 mg). After incubation for 1 h, TiO_2 beads were
137 washed [washing buffer 1; 80% (v/v) ACN, 1% (v/v) TFA, and washing buffer 2; 20% (v/v) ACN,
138 0.1% (v/v) TFA] and dried in a vacuum concentrator. Enzymatic deglycosylation of N-linked
139 sialoglycopeptides was performed with 1 µL of PNGase F for 3h at 37ºC. Released peptides were
140 recovered, dried, resuspended in 0.1% (v/v) TFA and then loaded on a LC-MS (AmaZon ETD Ion
141 Trap; Bruker Daltonik, Bremen, Germany) with an online-nanosprayer, and run as previously
142 described [34].

143

144 *Bioinformatics*

145 Acquired CID spectra were processed in DataAnalysis 4.0; deconvoluted spectra were further
146 analyzed with BioTools 3.2 software and submitted to Mascot database search (Mascot 2.2.04,
147 Swissprot database (546439 sequences; 194445396 residues, release date 19/20/14)). The
148 following variable modifications have been used: phosphorylation (STY), carbamidomethylation
149 (C), deamidation (NQ) and oxidation (M). To identify N-linked glycosylation sites, a deamidated
150 Asn residue had to be flanked by the glycosylation consensus motif (NXS/T, where X is any amino
151 acid besides proline) which was manually validated. Peptides that were assigned a deamidation
152 event based solely on the MS data (i.e., no *y*- or *b*- fragment ion for a particular deamidated Asn

153 residue could be detected) were presumed to be glycosylated only if a canonical N-glycan motif
154 was present.

155 The derived mass spectrometry datasets on the 3D-trap system were combined into protein
156 compilations using the ProteinExtractor functionality of Proteinscape 2.1.0 573 (Bruker Daltonics,
157 Bremen, Germany). In order to exclude false positive identifications, peptides with Mascot scores
158 below 40 were rejected. Peptides with a mascot score above 40 were manually validated in
159 BioTools (Bruker Daltonics, Bremen, Germany) on a residue-by residue basis using the raw data
160 to ensure accuracy as previously described [33]

161

162 *Peptide label-free quantification*

163 MS-based label-free quantification of the N-glycopeptides identified was performed using the
164 software Data Analysis 4.1 (Bruker Daltonik GmbH, Bremen, Germany). Peptides were matched
165 based on charge state, m/z value and elution time. The match was confirmed by visual inspection
166 of the peptide on the survey view and by manual comparison of the MS/MS spectra if available.
167 Relative peptide quantification was carried out by integrating the area of the extracted ion
168 chromatograms (XIC) of the monoisotopic peak from MS spectra (Fig. 1) [33]. For peptide
169 quantification, four biological replicates, each consisting of pooled samples from 3-4 mice, were
170 run.

171

172

173

174 *PLA_1 activity assay*

175 The phospholipase A_1 (PLA_1) activity of EL in intact mouse spermatozoa was analyzed using a
176 dye labeled-PLA_1 specific substrate [35]. Sperm samples were divided into six groups; non-
177 capacitated with or without H89 or A23187 and capacitated with or without H89 or A23187. The
178 compound H89 was supplemented 10 min prior to the addition of pentoxifylline and dbcAMP.
179 After capacitation for 1h, ionophore A23187 was added to cells (20 µM final concentration) after
180 30 min of incubation and then samples were allowed to incubate for another 30 min. Spermatozoa
181 were washed (300 x g, 3 min) twice using BWW media with BSA and then once with BWW media
182 without BSA. Sperm pellets were then resuspended in BWW media without BSA to a final
183 concentration of 20 x 10^6 sperm/ mL.

184 A stock solution of PED-A_1 substrate (5 mM in DMSO) was diluted (1:625) with BWW medium
185 without BSA yielding a final concentration of 8 µM. Aliquots of 25 µL of the PED-A_1 working
186 solution were placed in a v-bottom 96-well plate and then 25 µL of the sperm samples was added.
187 Controls included wells containing only PED-A_1 solution or sperm cells. The plate was incubated
188 at 37^{o}C and fluorescence measurements were taken every 30 sec during a 1h-period using the
189 microplate reader FLUOstar OPTIMA (BMG Labtech, Mornington, VIC, Australia) with
190 excitation and emission wavelengths of 485 and 510 nm, respectively. Linear regression was
191 calculated using the average results for the first 10 min of reading and reaction rates (slope) were
192 calculated for each sample. PLA_1 activity was assessed in five independent experiments.

193

194

195

196 Aconitase Vectors

197 ACO2 cDNA was ligated into the pcDNA3-EGFP plasmid. Primers were designed to have HindIII
198 (forward) and NotI (reverse) restriction sites as well as 8 extra base pairs on the ends to allow
199 enzyme cleavage. Two different reverse primers were used to create two different plasmids, the
200 first containing a linker sequence to create an ACO2-EGFP fusion, and the second containing a
201 linker sequence followed by a $(HIS)_6$-tag and stop codon to create his-tagged ACO2. This was
202 achieved using mouse cDNA and the following overhanging primers:

203 Forward: ACGAATTC–AAGCTT–ATGGCGCCTTACAGCCTCCTGGT
204 Reverse 1: GGTGCTTA–GCGGCCGC–GAGCTTCCACCACCTCC–
205 CTGCTGCAGCTCCTTCATCCTGTTG
206 Reverse 2: GGTGCTTA–GCGGCCGC–TCA–
207 ATGGTGGTGGTGATGATGGCTTCCACCACCTCC–
208 CTGCTGCAGCTCCTTCATCCTGTTG

209 For PCR, Thermo Scientific Phusion High-Fidelity DNA Polymerase was used and their
210 instructions followed. Each 20 µl PCR was made up with the following concentrations: 1 x HF
211 buffer, 200 µm dNTPs, 0.5 µM each of forward and reverse primer, ~100 ng DNA, 3% DMSO
212 and 1 unit Phusion polymerase. PCR conditions were: 98°C for 30 sec, [98°C for 10 sec, 65°C for
213 30 sec, 72°C for 2 min] x 35 cycles, 72°C for 10 min. Annealing temperature was optimized at
214 65°C for both sets of primers.

215 PCR inserts and pcDNA3-EGFP vector were digested with Promega enzymes; NotI and HindIII
216 after Wizard mini-prep kit clean-up. Insert and vector were ligated at a 3:1 ratio using Promega T4
217 DNA ligase and then transformed into E. coli cells on ampicillin agar plates. Singles colonies were

cultured the following day and then plasmids extracted. Plasmids were again digested with HindIII and NotI to check for insertions and the ones containing inserts were sent away for Sanger sequencing using four sequencing primers to cover entire insert and check for mutations: GGACTTTCCAAAATGTCG, AGGCCGAACAGACATTGC, AGATGCAGACGAGCTTCC, TTCATCCAGTGGACAAGC.

Site directed mutagenesis

To mimic the negative charge of the Sia modification on ACO2, we changed the amino acid 612 (Asn or N) to aspartic acid (D) using site directed mutagenesis. A single base pair change on chr15:81913178 to change the codon from AAC to GAC was achieved using the following primers:

Forward: TGCTCATCGGTGCCATCAACATC

Reverse: GGTTGTTAGAGATGTCATCCAGATGCCCAC

Phusion DNA Polymerase PCR was done using the same reaction as written in the above methods and the PCR conditions as follows: 98°C for 3 min, [98°C for 10 sec, 64 °C for 30 sec, 72°C for 6 min] x 35 cycles, 72°C for 10 min. Following PCR, the plasmid bands were cut out of an agarose gel, purified and digested with DpnI from NEB. Following another clean-up step, the plasmids were transformed into E. coli and grown on agar plates overnight. Single colonies were selected the following day and cultures grown overnight. Plasmids were extracted from these colonies and sent away for sequencing to check for mutation using sequencing primer AGATGCAGACGAGCTTCC.

239 *Transfection*

240 HEK293T cells were used for transfection with ACO2-EGFP plasmid and ACO2-$(HIS)_6$ plasmid
241 including the WT and N612D versions of these plasmids. We confirmed that human cells would
242 be suitable for transfection with the mouse ACO2 gene due to almost identical sequences. Cells
243 were split into 6-well plates to attain ~50% confluence the following day. Transfection was done
244 with 5 µg plasmid DNA and 10 µg PEI in 3 mL media. Firstly, 5 µg of plasmid and 10 µg PEI
245 were put into separate tubes and 150 µL DMEM (no FBS) added to each one. These were then
246 mixed together and incubated for 30 min. Next, media in the 6-well plates was replaced with 2.7
247 mL of fresh DMEM and the 300 µL DNA:PEI mix added. Cells were left to transfect for the times
248 indicated and then harvested. ACO2-GFP cells were fixed using 4% paraformaldehyde for
249 microscopy and FACS analysis or frozen at -80°C for immunoblotting. ACO2-$(HIS)_6$ cells were
250 frozen at -80°C for immunoblotting or Aconitase assay.

251

252 *Aconitase Assay*

253 Aconitase assay from BioVision was used with adjusted methods.

254 Day 1: Frozen transfected HEK293T cells consisting of $(HIS)_6$-wild-type ACO2 transfected (WT)
255 and N612D mutant and control non-transfected cells were thawed on ice. Cells were resuspended
256 in 400 mL lysis buffer (PBS pH 8, 10 mM imidazole, 0.5% tween) and then sonicated and
257 centrifuged (16,000 g, 4°C) for 15 min. A 200 µL aliquot of N612D and control samples were
258 placed in fresh tubes and the rest discarded. The WT samples were split into 3 tubes: 200 µL, 100
259 µL and 50 µL. A 200 µL of lysis buffer and then 50 µL Ni-NTA agarose beads were added and
260 samples rolled for 1 h at 4°C. Beads were washed thrice in wash buffer (PBS pH 8, 20 mM

imidazole, 0.5% tween) and once in kit assay buffer. Afterwards, beads were resuspended in 100 µL kit assay buffer, 10 µL activation solution was added, and samples were rolled for 1 h at 4°C. One hundred µL of reaction mix was added to each tube and samples rolled at room temperature overnight.

Day 2: Frozen non- and capacitated sperm cells were thawed on ice. Cells were resuspended in 100 µL kit assay buffer, sonicated and centrifuged (16,000 g; 4°C) for 15 min. Ten µL of activation solution was added and samples incubated for 1 h on ice. Afterwards, 100 µL reaction mix was added to each tube and samples incubated at room temperature for 2.5 h. Standards were made according to instructions and allowed to incubate for 30 min. The beads from day-1 preparation were centrifuged and, together with the non- and capacitated sperm prepared on day 2, were loaded in a 96-well plate in 100 µL duplicates. Ten µL of developer was added, samples incubated at room temperature 25°C and read at 450 nm.

Following kit, nickel bead enrichment, $(HIS)_6$-recombinant protein were eluted with 250 mM imidazole and then frozen along with non- and capacitated samples. For immunoblotting, samples were methanol/chloroform precipitated and lysed in SDS-PAGE buffer.

SDS-PAGE and immunoblotting

Non-capacitated and capacitated mouse spermatozoa (with and without H89) were prepared as described above and then diluted in SDS-PAGE buffer. Protein (10 µg) was separated by SDS-PAGE using 4-20% precast polyacrylamide gels (NuSep Ltd, Lane Cove, NSW, Australia) and then transferred onto nitrocellulose membrane Watman® Optitran® BA-S 85 (GE Healthcare, Castle Hill, NSW, Australia). The membrane was blocked (1 h at room temperature) and incubated

283 overnight at 4ºC with rabbit polyclonal antibody raised against EL (orb100394, LIPG; Biorbyt) at
284 a dilution of 1:500 in 5% (w/v) skim milk TBS-T (0.02 M Tris, 0.15 M NaCl, 0.1% (v/v) Tween-
285 20; pH 7.6).
286 After three washes, membrane was incubated for 1 h at room temperature with anti-rabbit IgG
287 horseradish peroxidase (HRP) conjugate (Sigma-Aldrich) at a concentration of 1:1000 in 5% (w/v)
288 skim milk TBS-T. The membrane was washed thrice, and immuno-reacted proteins were detected
289 using an enhanced chemiluminescence (ECL) kit (Amersham International) according to the
290 manufacturer's instructions. Equal loading was confirmed by stripping the membrane and then re-
291 probing it with a mouse monoclonal anti-α-tubulin antibody.
292 To confirm the capacitation of sperm cells and the efficiency of H89 at inhibiting tyrosine
293 phosphorylation via PKA, samples were probed with the mouse monoclonal anti-
294 phosphotyrosine–peroxidase antibody PT66 (A5964; Sigma-Aldrich). Loading control was
295 performed using mouse monoclonal anti-α-tubulin antibody.

296 Immunoblots of WT and mutant ACO2 were essentially performed as previously described [34].
297 The following antibody dilutions were used: rabbit polyclonal anti-Aconitase 2 antibody at 1:1000
298 (ab83528; Abcam), rabbit polyclonal anti-6X His tag antibody at 1:1000 (ab1187; Abcam). All
299 secondary antibodies were used at a 1:1000 dilution. Anti-GFP was a kind gift from Peter Lewis
300 and used at 1:1000.

301

302 *Immunocytochemistry*

303 Capacitated and non-capacitated intact mouse spermatozoa were fixed in 4% (w/v) formaldehyde
304 for 10 min at room temperature. Cells were washed three times in PBS containing 0.5 M glycine,

immobilized on poly-L-lysine coverslips and permeabilized with ice cold methanol for 10 min. Coverslips were washed, blocked for 1 h with 3% (w/v) BSA in PBS and incubated overnight with anti-EL antibody in a 1:50 dilution with PBS containing 1% (w/v) BSA. Following three washes with PBS, cells were incubated with Alexa Fluor® 488 goat anti-rabbit IgG (Life technologies) in a 1:100 dilution with PBS containing 1% (w/v) BSA. Coverslips were washed as described above and then mounted with Mowiol antifade medium. Cells were evaluated using phase contrast and epifluorescence microscopy.

Acrosomal status

The acrosomal status of mouse spermatozoa was assessed either at time 0 (non-capacitated) or following 30 min of capacitation (37°C; 5% CO2). After 30 min of incubation, the ionophore A23187 (10 µM final concentration in DMSO) or DMSO vehicle only were added and then cells were incubated for 30 min. Samples were washed twice using PBS and 10 µl of sperm suspension was spotted onto superfrost slides, spread with a glass pipette and air-dried. Slides were immersed in absolute methanol for 15 min, rinsed with PBS and then incubated for 30 min with fluorescein isothiocyanate-conjugated *Arachis hypogaea* peanut agglutinin (FITC-PNA) (15 µg/mL final concentration). The slides were rinsed in PBS and mounted with antifade media. For each slide, images of adjacent fields were recorded under a x40 magnification to achieve a sperm count of at least 100 spermatozoa. Spermatozoa were classified into one of the three categories of FITC-PNA labelling: I = intact acrosome; II = partial acrosome reaction; and III = complete acrosome reaction. For each experimental condition, a minimum of 3 slides were examined and quantified.

Statistical analysis

The data obtained by MS-based label-free quantification were normalized among runs using the average area of five different glycopeptides visually selected based on their quality and constant intensity. The normalized area of each glycopeptide was then compared between non-capacitated and capacitated sperm samples using student's *t*-test. Relative immunoreactivity for EL and α-tubulin and sperm PLA_1 activity were compared among groups using paired *t*-test. P-values < 0.01 were considered as significant. Standard errors are shown in the graphs. The data for acrosome reaction from 5 biological replicates were subjected to analysis of variance (two-way ANOVA) followed by paired *t*-test. Data are shown as mean ± S.D. when not specified otherwise.

Molecular modelling; Covalent docking model of Sialic acid binding of Asn612 to aconitate hydratase

Molecular docking experiments were carried out using the program GOLD (Genetic Optimization for Ligand Docking) version 5.2 and favouring the CHEMPLP Scoring system (Verdonk 2003). The three-dimensional iteration of Sialic acid (MolPort-008-267-866) was used for covalent docking onto the identified target residue of Asn612 on a model of Aconitate hydratase, mitochondrial precursor from *Mus musculus* (EC: 4.2.1.3) generated by the PHYRE2 protein recognition server Kelley (2015). The proposed reaction mechanism and subsequent product is depicted in Scheme 1. The size of the search domain was set to 10 Å and the covalent docking function within GOLD was employed. Docking was executed using a 100% search efficiency, generating ten Genetic Algorithm (GA) runs, while the rotameric states of several sidechains including Gln563, Lys605 and Arg648 were set to library rotamer orientations and the remainder

of the site remained rigid. The generated binding poses were then inspected, and conformations were chosen for further analysis taking into account their ranking and interactions with the probed residues**.** Molecular visualizations were performed using the software package PYMOL (Schrödinger, NY, USA).

Results

In order to determine the efficiency of the protocol used here to induce sperm capacitation, tyrosine phosphorylation was measured (Fig. 1). As shown, tyrosine phosphorylation increased during capacitation, which could be abrogate with the PKA inhibitor H89, suggesting that the sperm cells used in this study were capacitating. The experimental paradigm used in this study was to compare the changes associated with the capacitation process itself (Cap *vs* Cap-H, Fig. 2) as opposed to changes over time (N-Cap *vs* Cap, Fig. 2).

Sialylated glycoproteins identified in mouse sperm

The protocol to enrich for sialylated N-linked glycopeptides is shown in Figure 2. Herein, spermatozoa were obtained from the mouse epididymides, combined, and then separated into two separate tubes. Whilst one tube had capacitating media, the other lacked sodium bicarbonate which is essential for this process. The samples were washed, lysed and digested. Sialylated-glycoprotein enrichment was performed using TiO_2 beads. Although this is not specific for glycopeptides, but rather for negatively charged molecules, the elution through PNGase F treatment of the beads allows the selection of N-linked glycopeptides generally or sialylated glycopeptides specifically.

Enrichment of sialylated N-linked glycopeptides using TiO_2 allowed the identification of 142 unique peptides, which were from 90 different glycoproteins (Table 1), demonstrating that some proteins possessed N-linked glycopeptides with terminal Sia in more than one position. Of particular interest, the characterization of the glycopeptides containing Sia residues represented 36.7% of the total non-reductant peptides identified by MS/MS. This is in perfect agreement with our previous paper with rat sperm, in which around 34% of the peptides identified were classified as glycopeptides after enrichment using TiO_2 [33].

Due to ion fragmentation patterns (i.e., no visualization of the *y*- or *b*- fragment ion for the deamidated Asn), a precise identification of the residue containing the deamidation was not possible in all cases. Hence, the peptides exhibiting ambiguous annotation of the deamidated residue are indicated in Table 1 with an asterisk. Supplementary I contains MS/MS spectrum from all peptides present in Table 1 whereas Supplementary II presents data such as measured m/z values, peptide charge and retention times.

Changes in sialylated N-linked glycopeptides during capacitation

The data for label-free quantification of the N-linked glycopeptides in non-capacitated versus capacitated sperm are shown in Table 1. Some glycopeptides were presented at very low amount, impairing their quantification in some biological replicates. These cases are indicated in Table 1 as not determined (ND) since we were not confident to report these further. Of interest, nine (6.3%) of the glycopeptides identified here underwent significant changes during sperm capacitation. These glycopeptides belong to the proteins: ACO2, C4b-binding protein (C4BP), EL, inactive serine protease 39 (PRSS39, also known as testicular-specific serine protease 1; TESP1), serine

392 protease 52 (PRSS52, also known as testicular-specific serine protease 3; TESP3), testis-expressed
393 protein 101 (TEX101) and zonadhesin (Table 1). Interesting, these glycopeptides were shown to
394 be reduced during capacitation except for the peptide from ACO2, a protein involved in the
395 tricarboxylic acid (TCA) cycle (Table 1).

396

397 *Determination of EL amount and sub-cellular localization*

398 In order to determine the consequences of sialylation changes during capacitation, we choose two
399 proteins for further study: the EL and ACO2. The EL has been reported as primarily having PLA_1
400 activity [36]. This was of particular interest, since changes in the composition of lipids from cell
401 membranes, such as the formation of lysophospholipids by phospholipids hydrolysis, are known
402 to modify membrane fluidity [37, 38] and function through the modulation of receptors [39],
403 channels [40, 41] and enzyme activity [42] within its structure. Considering that morphological
404 and functional changes in sperm membranes, including alteration in membrane fluidity, are
405 essential for capacitation [43] and that lysophospholipids may be involved in the modulation of
406 the acrosome reaction [44], we further investigated the behavior of EL during this process.

407 Immunoblotting for EL was performed, aiming to determine what happens to the entire protein
408 during capacitation. As shown in Figure 3, the total amount and the molecular weight of EL did
409 not change after capacitation (Fig. 3A, lanes 1 and 2). In addition, the use of the PKA inhibitor
410 H89 during capacitation also did not affect the amount of EL (Fig. 3A, lanes 2 and 3). To
411 demonstrate equal loading, we re-probed the sample with anti-α tubulin antibody (Fig. 3B). Using
412 the software Image J, the quantitative values of each band were plotted to confirm that no
413 significant change occur in EL expression after capacitation (Fig. 3C).

To verify whether the protein EL is redistributed in spermatozoa during capacitation, we performed immunostaining using anti-EL antibody. Immunostaining for EL was observed in both head and tail regions of non-capacitated (Fig. 4a,c) and capacitated (Fig. 4b,d) mouse sperm. For both groups, the anterior acrosome region stained for EL whereas the equatorial region showed no staining. In addition, the staining intensity of the postacrosomal sheath showed high variation among cells; being absent in some cases (Fig. 4b, white arrow exemplifies this variation). In the tail region, although the midpiece and the cytoplasmic droplet showed high staining for EL, we noted that some cells exhibited weaker labeling of the midpiece (Fig. 4c,d). Of interest, the percentage of these cells, with reduced immunoreactivity for EL at the midpiece, increased when sperm was incubated in capacitating conditions (from around 7% to 68%). The same was observed in samples capacitated with the PKA inhibitor H89, suggesting that the diminish in EL immunofluorescence within the midpiece is independent of PKA (data not shown). Secondary only controls showed no fluorescence (Fig. 4e,f).

Loss in EL activity occurs during capacitation, independent of H89 and the acrosome reactions

In order to determine if the loss of Sia residue on EL affected enzyme activity, we specifically measured PLA_1 activity on both non- and capacitated spermatozoa. Furthermore, as the immunofluorescence showed quite a varied pattern of EL expression, including acrosome location, we wanted to see if the loss of the acrosome had any effect of the overall EL activity. Therefore, we incubated sperm under non- or capacitating condition, with and without H89. Secondly, both non- and capacitated spermatozoa were induced to undergo the acrosome reaction. These sperm cells were subsequently washed, then the level of intact, partial or complete acrosome loss were

436 measured using FITC-PNA staining. As shown in Figure 5, capacitated sperm plus ionophore
437 A23187 had the highest level of complete acrosomal loss as expected.

438 To determine whether a change in EL activity occurred during capacitation, we measured PLA_1
439 activity before and after capacitation, together with the inhibitor H89 or the acrosomal-inducer,
440 ionophore A23187. We observed a significant loss in the PLA_1 activity of EL during capacitation
441 (Fig. 6A, bars N-cap *vs* Cap). An example of the loss in PLA_1 activity is demonstrated in Figure
442 6B. Here, two of the five biological replicates are shown over time from either non-capacitated
443 (solid line) or capacitated (dotted line) sperm populations. Addition of the PKA inhibitor H89,
444 which is commonly used to prevent capacitation, failed to abrogate the loss of PLA_1 activity (Fig.
445 6A, N-cap + H89 *vs* Cap + H89). Furthermore, the loss of the acrosome had no further bearing on
446 the reduction of the PLA_1 activity in EL, with acrosome-reacted capacitated spermatozoa (Fig. 6A,
447 bar Cap + A23187) having a similar activity to the capacitated (Fig. 6A, bar Cap) and the H89
448 "capacitated" (Fig. 6A, Cap + H89) cells. In all cases, the amount of activity was normalized to
449 the amount of endothelial lipase present with an immunblot.

450

451 *Sialylation of N612 inhibits ACO2 activity*

452 Spermatozoa are catabolic in nature and, as such, it is not a surprise that the majority of Sia residues
453 are lost during capacitation. However, in this study, we observed one enzyme that had an increase
454 in sialylation, namely ACO2. To further understand this finding, we measured total Aconitase
455 activity before and following mouse capacitation. As shown, during capacitation a statistically
456 significant decrease in the level of Aconitase activity was observed (Fig. 7). Although this
457 measurement would include both cytoplasmic and mitochondrial Aconitase activity, we reasoned

458 that sperm have very little cytoplasm, therefore, the bulk of Aconitase activity should be from the
459 mitochondrial form.

460 To confirm that a decrease in ACO2 activity occurs specifically through sialylation at N612, we
461 made both WT and Sia mimic, whereby the N612 was replaced by the negatively charged Aspartic
462 acid (N612D). In both cases (WT and mimic), we made a GFP- and a HIS-tagged separate proteins.

463 Expression of the GFP-tagged proteins showed both WT and mutant were expressed in the
464 mitochondria as expected (Fig. 8A-D). Of interest, under fluorescence microscopy, we also noted
465 a decrease in the level of GFP-tagged mutant, yet the number of cells transfected was equal
466 (compare Fig. 8A and 8B). To support this, we ran the cells through flow-cytometry. Analysis
467 demonstrated that, in every replicate, the same number of cells were transfected (on average 35%),
468 however, the mean level of GFP-fluorescence was significantly lower in the N612E-Aconitase
469 expressing cells. For example, the histogram on Figures 8C and 8D demonstrates that the peak
470 height for GFP fluorescence in WT is slightly higher (Fig. 8E, black downward arrow) than in the
471 N612E mutant (Fig. 8F, black downward arrow). This suggests that cells are less favorable to the
472 expression of the N612E mutant over the WT. To confirm this hypothesis, we ran a SDS gel,
473 transferred and probed it with antibodies against GFP- (not shown) or $(His)_6$-tagged proteins (Fig.
474 9A,B). As shown, WT ACO2 is more abundant than the mutant form (Fig. 9A,B; compare lanes 1
475 to 4). From our estimation, the N612E expression is between 25-50% of that of WT (see lanes 3
476 and 4 *vs* 5).

477 We next measured the ACO2 activity of the WT and N612E mutant (Fig. 10). The use of equal
478 amounts of recombinant protein was confirmed by immunoblotting. Remarkably, even when left
479 overnight, we were unsuccessful in obtaining any ACO2 activity from the N612E mutant. In

480 contrast, we could easily detect WT ACO2 activity. When put together, these datasets suggest that
481 a switch in the ACO2 activity occurs during capacitation. This change in activity pattern is likely
482 related to the modifications in the metabolic pathways described during the capacitation of mouse
483 spermatozoa (i.e., from the oxidative phosphorylation pathway to the glycolytic pathway).

484 *Modelling the bound sialoglycoprotein to Aconitate hydratase*

485 To understand the impact sialation would have on N612, we modelled the effect. Published crystal
486 structures of Aconitate hydratase [45-48] and our highly homologous model, describes a large
487 macromolecular structure comprising of four distinct domains employing a [4Fe-4S] cluster to
488 catalyse the stereospecific dehydration of citrate to isocitrate [49]. Within the enzyme itself, sits
489 several highly conserved amino acids, such as Asp192, His194 and Arg607 that are crucial for
490 ACO2 activity (shown in Fig. 11). N612 resides on a short α-helical element immediately atop the
491 active site, in an area often denoted as domain 4 [50]. In order to fit a sialic acid residue with N612,
492 multiple changes in rotamers of sidechains were required. This allowed the formation of new salt
493 bridges and hydrogen bonds between the sugar and the α-helical structure including the residue
494 N614 (Asn615) and Gln563 which is present on an adjacent loop (Fig 11A,B). This data suggest
495 that inhibition of Aconitase activity, through siltation of Aspargine 612, is due to major distortion
496 of the active site which prevents catalysis from occurring.

497

498 **Discussion**

499 Despite the importance of capacitation, the molecular mechanisms underlying this process are not
500 yet fully understood. Previous studies have suggested that one facet of capacitation is a loss in Sia
501 residues, which may be modulated by one (humans) or two (mouse) neuraminidases, namely

neuraminidase 1 and 3 [27]. In the present study, using a LC-MS/MS-based approach, we were able to investigate capacitation-related changes of N-linked glycoproteins bearing terminal Sia. Surprisingly, we found very little regulation of Sia within proteins groups following *in vitro* capacitation, with only 6.3% (9 of 142 peptides) demonstrating a significant change.

According to our data, the enzyme EL is one of the sperm proteins in which the Sia content is altered during capacitation. Previous studies have shown that four (N62, N118, N375, and N473) of the five potential N-glycosylation sites of human EL are occupied by glycan moieties [51, 52]. In the present study, the sugar moiety at the N62 glycosylation site of EL was found to contain Sia in its structure. In addition, the peptide containing this glycosylation site was significantly reduced after *in vitro* capacitation, despite the fact that both quantity and molecular weight of EL remained unchanged. This suggests that a loss of a small glycan moiety or of a Sia residue itself occurs within EL during capacitation. Notably, a sialylated N-glycan structure at the corresponding glycosylation site (N64) has also been identified by our group in the EL of rat sperm [33]. In this case, spermatozoa were taken from the caput, corpus and cauda regions of the epididymis. Remarkably, the Sia residue within EL was only found in spermatozoa derived from the caudal location. Furthermore, we have observed that the amount of EL within rat spermatozoa does not change, suggesting that Sia is added to EL during epididymal transit (**data not published;** [33]). Given that Sia residues are removed from the same glycosylation site during capacitation, it is likely that this glycan moiety plays a specific role in regulating EL enzyme activity.

The glycosylation site at N62 of mouse EL is a conserved feature among animals and other members of the triglyceride lipase gene family, such as lipoprotein lipase and hepatic lipase. Using recombinant proteins, two separate studies have produced point mutations of the amino acids that are glycosylated in EL. Interestingly, in both cases, the loss of N62 led to increased EL activity

525 [51, 52]. Due to their negative charge and hydrophilicity, Sia residues within this glycan moiety
526 could influence the structure and/or substrate specificity of EL, therefore, regulating its enzymatic
527 activity. Of note however, we observed a decrease in the PLA_1 activity of EL following reduction
528 of its sialylated glycopeptides (N62 glycosylation site) during capacitation. We can only assume
529 that, besides the loss of N62, EL is likely to be regulated in other (as yet unknown) ways in order
530 to switch off its activity.

531 In addition to EL, we found N612 sialytion of ACO2 increase following *in vitro* capacitation. This
532 enzyme catalyzes the non-redox reaction of the TCA cycle in which stereo-specific isomerization
533 of citrate to isocitrate occurs [53]. Adequate supply of ATP is essential to support capacitation-
534 associated changes such as hyperactivation [54]. In mouse, it is fairly well understood that, during
535 capacitation, there is a switch from oxidative phosphorylation over to glycolysis [5]. Thus, non-
536 capacitated sperm show high oxygen consumption, which diminishes as sperm make the switch
537 over to glycolysis during capacitation [5]. Herein, such a switch could be brought about through
538 sialylation of ACO2 particularly N612. Indeed, modelling of the enzyme suggests that the Asn
539 group sits atop of the ACO2 activity site (Fig. 11) in a highly conserved region. Analyses of
540 multiple X-ray crystal structures of Aconitate hydratase has shown that a vast array of residues
541 from all four domains of the enzyme are required to carry out catalysis [55] whether it's to bind
542 and recognize substrate or ligate the [4Fe-4S] cluster. Similarly, this complex array, dependent on
543 bound ligands, displays a number of nuanced and obvious conformational changes within its active
544 site and other domains [55]. Thus, it is apparent that in our model, inhibition likely occurs through
545 segmental conformational change of the antiparallel helical motif that N612 is a part (residues 606-
546 612 in our model; Fig. 11). As this includes active site residue Arg607, it is possible changes in
547 substrate binding may occur to prevent catalysis such as a rotameric shifts or larger domain

548 movements that may prevent substrate binding and release, a trait often linked with N-linked
549 glycosylation [56]. With the observation that both the mutation to Glutamate (Glu612) and the
550 Asn612 sialic acid (N-link) modified enzymes shuts down activity of the enzyme and the former
551 modification in our models (not depicted) suggests a new salt bridge or hydrogen bond with the
552 either the sidechain amine of Gln563 or Lys605 is likely. This further underlines the potential
553 sensitivity of ACO2 activity with respect to changes to this motif with the potential they instigate
554 larger downstream changes in other domains.

555 Inspection of Uniprot suggests that the glycosylation at N612 has never been reported in
556 any other cell type and, as such, may represent a novel mechanism, attributed just to sperm cells.
557 Unfortunately, compounds to block or inhibit sialic acid transferases are not cell permeable and,
558 for this reason, we were unable to directly ascribe the significance of a lack of ACO2 activity to
559 sperm physiology. Additionally, an indiscriminate blockage of sialyltransferases would have
560 raised doubts about what other proteins/pathways could also have been co-inhibited and this
561 obfuscated the interpretation. Our leading hypothesis is that glycolysis is required for the rapid
562 movement of the sperm flagella, in a process known as hyperactivation. The latter being essential
563 for fertilization to occur. Therefore, sperm cells being transcriptionally and translationally silent
564 cells may change ACO2 activity via sialylation of this protein, which facilitates the shuttling of its
565 metabolic process from oxidative phosphorylation over to glycolysis.

566

567 **References**

568

569

1. Chang MC: **Fertilizing capacity of spermatozoa deposited into the fallopian tubes**. *Nature* 1951, **168**(4277):697-698.
2. Visconti PE, Bailey JL, Moore GD, Pan D, Olds-Clarke P, Kopf GS: **Capacitation of mouse spermatozoa. I. Correlation between the capacitation state and protein tyrosine phosphorylation**. *Development* 1995, **121**(4):1129-1137.
3. Visconti PE, Moore GD, Bailey JL, Leclerc P, Connors SA, Pan D, Olds-Clarke P, Kopf GS: **Capacitation of mouse spermatozoa. II. Protein tyrosine phosphorylation and capacitation are regulated by a cAMP-dependent pathway**. *Development* 1995, **121**(4):1139-1150.
4. Baker MA: **Proteomics of post-translational modifications of mammalian spermatozoa**. *Cell and tissue research* 2016, **363**(1):279-287.
5. Fraser LR, Lane M: **Capacitation-and fertilization-related alterations in mouse sperm oxygen consumption**. *Reproduction* 1987, **81**(2):385-393.
6. Miki K, Qu W, Goulding EH, Willis WD, Bunch DO, Strader LF, Perreault SD, Eddy EM, O'Brien DA: **Glyceraldehyde 3-phosphate dehydrogenase-S, a sperm-specific glycolytic enzyme, is required for sperm motility and male fertility**. *Proceedings of the National Academy of Sciences* 2004, **101**(47):16501-16506.
7. Baker MA: **The'omics revolution and our understanding of sperm cell biology**. *Asian journal of andrology* 2011, **13**(1):6.
8. Baker MA, Nixon B, Naumovski N, Aitken RJ: **Proteomic insights into the maturation and capacitation of mammalian spermatozoa**. *Systems biology in reproductive medicine* 2012, **58**(4):211-217.
9. Ficarro S, Chertihin O, Westbrook VA, White F, Jayes F, Kalab P, Marto JA, Shabanowitz J, Herr JC, Hunt DF: **Phosphoproteome analysis of capacitated human sperm evidence of tyrosine phosphorylation of a kinase-anchoring protein 3 and valosin-containing protein/p97 during capacitation**. *Journal of Biological Chemistry* 2003, **278**(13):11579-11589.
10. Porambo JR, Salicioni AM, Visconti PE, Platt MD: **Sperm phosphoproteomics: historical perspectives and current methodologies**. *Expert review of proteomics* 2012, **9**(5):533-548.
11. Brewis IA, Gadella BM: **Sperm surface proteomics: from protein lists to biological function**. *MHR: Basic science of reproductive medicine* 2009, **16**(2):68-79.
12. Varki A: **Biological roles of oligosaccharides: all of the theories are correct**. *Glycobiology* 1993, **3**(2):97-130.
13. Lowe JB, Marth JD: **A genetic approach to mammalian glycan function**. *Annual review of biochemistry* 2003, **72**(1):643-691.
14. Fei W, Hao X: **Wheat germ agglutinin (WGA) receptors on human sperm membrane and male infertility**. *Archives of andrology* 1990, **24**(1):97-97.
15. Jiménez I, Gonzalez-Marquez H, Ortiz R, Betancourt M, Herrera J, Fierro R: **Expression of lectin receptors on the membrane surface of sperm of fertile and subfertile boars by flow cytometry**. *Archives of andrology* 2002, **48**(2):159-166.
16. Steele M, Wishart G: **Demonstration that the removal of sialic acid from the surface of chicken spermatozoa impedes their transvaginal migration**. *Theriogenology* 1996, **46**(6):1037-1044.
17. Yudin AI, Generao SE, Tollner TL, Treece CA, Overstreet JW, Cherr GN: **Beta-defensin 126 on the cell surface protects sperm from immunorecognition and binding of anti-sperm antibodies**. *Biology of reproduction* 2005, **73**(6):1243-1252.
18. Ma X, Pan Q, Feng Y, Choudhury BP, Ma Q, Gagneux P, Ma F: **Sialylation facilitates the maturation of mammalian sperm and affects its survival in female uterus**. *Biology of reproduction* 2016, **94**(6):123, 121-110.

19. Tollner TL, Yudin AI, Treece CA, Overstreet JW, Cherr GN: **Macaque sperm coating protein DEFB126 facilitates sperm penetration of cervical mucus**. *Human reproduction* 2008, **23**(11):2523-2534.
20. Focarelli R, Giuffrida A, Rosati F: **Changes in the sialylglycoconjugate distribution on the human sperm surface during in-vitro capacitation: partial purification of a 20 kDa sialylglycoprotein of capacitated spermatozoa**. *MHR: Basic science of reproductive medicine* 1995, **1**(8):369-373.
21. Mahmoud A, Parrish J: **Oviduct fluid and heparin induce similar surface changes in bovine sperm during capacitation: a flow cytometric study using lectins**. *Molecular Reproduction and Development: Incorporating Gamete Research* 1996, **43**(4):554-560.
22. Medeiros C, Parrish J: **Changes in lectin binding to bovine sperm during heparin-induced capacitation**. *Molecular Reproduction and Development: Incorporating Gamete Research* 1996, **44**(4):525-532.
23. Jiménez I, González-Márquez H, Ortiz Ro, Herrera JA, García A, Betancourt M, Fierro R: **Changes in the distribution of lectin receptors during capacitation and acrosome reaction in boar spermatozoa**. *Theriogenology* 2003, **59**(5-6):1171-1180.
24. Rosado A, Velázquez A, Lara-Ricalde R: **Cell polarography. II. Effect of neuraminidase and follicular fluid upon the surface characteristics of human spermatozoa**. *Fertility and sterility* 1973, **24**(5):349-354.
25. Iqbal N, Hunter A: **Comparison of various bovine sperm capacitation systems for their ability to alter the net negative surface charge of spermatozoa**. *Journal of dairy science* 1995, **78**(1):84-90.
26. Focarelli R, Rosati F, Terrana B: **Sialylglycoconjugates release during in vitro capacitation of human spermatozoa**. *Journal of andrology* 1990, **11**(2):97-104.
27. Ma F, Wu D, Deng L, Secrest P, Zhao J, Varki N, Lindheim S, Gagneux P: **Sialidases on mammalian sperm mediate deciduous sialylation during capacitation**. *Journal of Biological Chemistry* 2012, **287**(45):38073-38079.
28. Davis BK, Byrne R, Bedigian K: **Studies on the mechanism of capacitation: albumin-mediated changes in plasma membrane lipids during in vitro incubation of rat sperm cells**. *Proceedings of the national academy of sciences* 1980, **77**(3):1546-1550.
29. Baker MA, Krutskikh A, Curry BJ, McLaughlin EA, Aitken RJ: **Identification of cytochrome P450-reductase as the enzyme responsible for NADPH-dependent lucigenin and tetrazolium salt reduction in rat epididymal sperm preparations**. *Biology of reproduction* 2004, **71**(1):307-318.
30. Baker MA, Krutskikh A, Curry BJ, Hetherington L, Aitken RJ: **Identification of cytochrome-b5 reductase as the enzyme responsible for NADH-dependent lucigenin chemiluminescence in human spermatozoa**. *Biology of reproduction* 2005, **73**(2):334-342.
31. Daniel Jr J: **Methods in mammalian embryology**. *Methods in mammalian embryology* 1971.
32. Wessel D, Flugge UI: **A method for the quantitative recovery of protein in dilute solution in the presence of detergents and lipids**. *Anal Biochem* 1984, **138**(1):141-143.
33. Villaverde AISB, Hetherington L, Baker MA: **Quantitative glycopeptide changes in rat sperm during epididymal transit**. *Biology of reproduction* 2016, **94**(4):91, 91-13.
34. Baker MA, Naumovski N, Hetherington L, Weinberg A, Velkov T, Aitken RJ: **Head and flagella subcompartmental proteomic analysis of human spermatozoa**. *Proteomics* 2013, **13**(1):61-74.
35. Darrow AL, Olson MW, Xin H, Burke SL, Smith C, Schalk-Hihi C, Williams R, Bayoumy SS, Deckman IC, Todd MJ: **A novel fluorogenic substrate for the measurement of endothelial lipase activity**. *Journal of lipid research* 2011, **52**(2):374-382.
36. McCoy MG, Sun G-S, Marchadier D, Maugeais C, Glick JM, Rader DJ: **Characterization of the lipolytic activity of endothelial lipase**. *Journal of lipid research* 2002, **43**(6):921-929.

37. Seu KJ, Cambrea LR, Everly RM, Hovis JS: **Influence of lipid chemistry on membrane fluidity: tail and headgroup interactions**. *Biophysical journal* 2006, **91**(10):3727-3735.
38. Dawaliby R, Trubbia C, Delporte C, Noyon C, Ruysschaert J-M, Van Antwerpen P, Govaerts C: **Phosphatidylethanolamine is a key regulator of membrane fluidity in eukaryotic cells**. *Journal of Biological Chemistry* 2016, **291**(7):3658-3667.
39. McCallum CD, Epand RM: **Insulin receptor autophosphorylation and signaling is altered by modulation of membrane physical properties**. *Biochemistry* 1995, **34**(6):1815-1824.
40. Inoue N, Hirata K, Yamada M, Hamamori Y, Matsuda Y, Akita H, Yokoyama M: **Lysophosphatidylcholine inhibits bradykinin-induced phosphoinositide hydrolysis and calcium transients in cultured bovine aortic endothelial cells**. *Circulation research* 1992, **71**(6):1410-1421.
41. Lundbaek JA, Andersen OS: **Lysophospholipids modulate channel function by altering the mechanical properties of lipid bilayers**. *The Journal of general physiology* 1994, **104**(4):645-673.
42. Owens K, Kennett FF, Weglicki WB: **Effects of fatty acid intermediates on Na+-K+-ATPase activity of cardiac sarcolemma**. *American Journal of Physiology-Heart and Circulatory Physiology* 1982, **242**(3):H456-H461.
43. Salicioni AM, Platt MD, Wertheimer EV, Arcelay E, Allaire A, Sosnik J, Visconti PE: **Signalling pathways involved in sperm capacitation**. *Society of Reproduction and Fertility supplement* 2007, **65**:245.
44. Roldan E, Shi Q: **Sperm phospholipases and acrosomal exocytosis**. *Front Biosci* 2007, **12**(1):89-104.
45. Lloyd S, Lauble H, Prasad G, Stout C: **The mechanism of aconitase: 1.8 Å resolution crystal structure of the S642A: citrate complex**. *Protein Science* 1999, **8**(12):2655-2662.
46. Lauble H, Kennedy M, Emptage M, Beinert H, Stout C: **The reaction of fluorocitrate with aconitase and the crystal structure of the enzyme-inhibitor complex**. *Proceedings of the National Academy of Sciences* 1996, **93**(24):13699-13703.
47. Lauble H, Kennedy MC, Beinert H, Stout CD: **Crystal structures of aconitase with trans-aconitate and nitrocitrate bound**. *Journal of molecular biology* 1994, **237**(4):437-451.
48. Robbins A, Stout C: **Structure of activated aconitase: formation of the [4Fe-4S] cluster in the crystal**. *Proceedings of the National Academy of Sciences* 1989, **86**(10):3639-3643.
49. Beinert H, Kennedy MC, Stout CD: **Aconitase as iron– sulfur protein, enzyme, and iron-regulatory protein**. *Chemical reviews* 1996, **96**(7):2335-2374.
50. Dupuy J, Volbeda A, Carpentier P, Darnault C, Moulis J-M, Fontecilla-Camps JC: **Crystal structure of human iron regulatory protein 1 as cytosolic aconitase**. *Structure* 2006, **14**(1):129-139.
51. Miller GC, Long CJ, Bojilova ED, Marchadier D, Badellino KO, Blanchard N, Fuki IV, Glick JM, Rader DJ: **Role of N-linked glycosylation in the secretion and activity of endothelial lipase**. *Journal of lipid research* 2004, **45**(11):2080-2087.
52. Skropeta D, Settasatian C, McMahon MR, Shearston K, Caiazza D, McGrath KC, Jin W, Rader DJ, Barter PJ, Rye K-A: **N-Glycosylation regulates endothelial lipase-mediated phospholipid hydrolysis in apoE-and apoA-I-containing high density lipoproteins**. *Journal of lipid research* 2007, **48**(9):2047-2057.
53. Beinert H, Kennedy MC: **Aconitase, a two-faced protein: enzyme and iron regulatory factor**. *The FASEB journal* 1993, **7**(15):1442-1449.
54. Ferramosca A, Zara V: **Bioenergetics of mammalian sperm capacitation**. *BioMed research international* 2014, **2014**.
55. Lauble H, Stout CD: **Steric and conformational features of the aconitase mechanism**. *Proteins: Structure, Function, and Bioinformatics* 1995, **22**(1):1-11.

56. Imperiali B, O'Connor SE: **Effect of N-linked glycosylation on glycopeptide and glycoprotein structure**. *Current opinion in chemical biology* 1999, **3**(6):643-649.

Figure Legends:

Figure 1. Immunoblotting of mouse cauda sperm previously incubated in non-capacitating (N-Cap) or capacitating media supplemented (Cap-H) or not (Cap) with the PKA inhibitor H89. Protein extraction was performed in SDS-PAGE buffer and 10 µg was loaded per lane. Membranes were probed with anti-Phosphotyrosine PT66 antibody and then re-probed with anti-α-tubulin. The data show one replicate that has been repeated in 6 biological replicates.

Figure 2. Schematic representation of the strategy used to identify and quantify sialylated N-linked glycopeptides extracted from mouse sperm. Deamidated asparagine residue (-D).

Figure 3. Immunoblot analysis of cauda spermatozoa from mouse. Sperm samples were incubated in non-capacitating (N-Cap) or capacitating media supplemented (Cap-H) or not (Cap) with the PKA inhibitor H89. Extraction was performed using SDS-PAGE buffer and 15 µg of protein was loaded per lane. **(A)** Membranes were probed with anti-EL and then **(B)** re-probed with anti-α-tubulin. **(C)** Graphic below shows relative immunoreactivity levels of both EL (left) and α-tubulin (right). No statistical difference was observed among groups, which consist of five biological replicates each.

733 **Figure 4**. Immunofluorescent localization of EL and the corresponding phase-contrast
734 micrographs of non-capacitated and capacitated mouse sperm cells. (**a-d'**) Fixed spermatozoa were
735 immobilized on pre-coated slides, permeabilized with ice cold methanol and incubated overnight
736 with anti-EL antibody. Alexa Fluor 488-conjugated secondary antibody was used for detection of
737 the primary antibody. Primary antibody was omitted in control (e and f). The scale bars represent
738 20 μm. The experiment was repeated using four biological replicates.

739

740 **Figure 5**. Assessment of acrosomal status by FITC-PNA labelling of non-capacitated (black and
741 grey bars) and capacitated (hatched and dotted bars) mouse sperm either with (grey and dotted
742 bars) or without (black and hatched bars) previous incubation with calcium ionophore A23187.
743 Sperm were counted for intact, partial or complete acrosome reaction. The data were expressed as
744 mean ± SE. Different letters represent statistical differences ($p < 0.01$) between treatments within
745 each category (intact, partial or complete acrosome reaction). The graph represents the average of
746 5 biological replicates.

747

748 **Figure 6.** Phospholipase A_1 (PLA_1) activity and the effect of the addition of A23187 and the PKA
749 inhibitor H89 on non- and capacitated mouse spermatozoa. Enzyme activity was measured using
750 the fluorescent PED-A_1 substrate. **(A)** PLA_1 activity rate, within the first 10 min, for sperm cells
751 previously incubated in non-capacitating or capacitating media with or without H89 and A23187.
752 Image represents the mean value of five biological experiments. **(B)** Example of the raw data for
753 two non-capacitated (solid line) and two capacitated (dotted line) samples.

754

Figure 7. Decrease in Aconitase activity during capacitation. Spermatozoa from mice were retrieved and incubated under non- or capacitating conditions. Following protein extraction, Aconitase activity was measured. To ensure equal amounts of Aconitase were present, the lysate was precipitated, run into SDS page, transferred and probed using anti-Aconitase antibody. The data shown is the average (± SD) of four biological replicates. Asterisk represents statistical significance ($p < 0.01$).

Figure 8. Following cloning and insertion of the Aconitase gene into plasmid, site directed mutagenesis was used to create the N612E mutant. **(A-D)** HEK293 cells were transiently transfected with GFP-tagged WT **(A,C)** or N612E mutant **(B,D).** Both anti-GFP tag fluorescent **(A,B)** and phase **(C,D)** images were taken. Scale bar = 50 μM. **(E-F)** Transfected cells were run through flow cytometer. Shown is the FL-1 channel vs counts of **(E)** GFP-tagged WT or **(F)** GFP-tagged N612E mutant. Arrow points to the mean signal intensity for each sample. Horizontal line represents the gate used for cell counting. **(G)** shows signal from non-transfected cells**.**

Figure 9. HEK293 cells were transfected with either $(His)_6$-tagged WT or $(His)_6$-tagged N612E mutant for Aconitase. Cells were lysed and recombinant Aconitase purified on nickel beads. Following elution, samples were run and probed with **(G)** anti-$(His)_6$-tagged protein or **(H)** anti-Aconitase. Control samples comprise non-transfected cells.

Figure 10. N612E-mutant Aconitase displays no activity**.** HEK293 cells were transiently transfected with $(His)_6$-tagged WT and $(His)_6$-tagged N612E mutant. Aconitase was purified over nickel beads, run in SDS-PAGE and the immunoblotting performed to ensure that equal amounts of protein were used. Bars demonstrate the average (n=6) activity of Aconitase with SD. Non-transfected cells were used as controls.

Figure 11. (A) Ball and stick together with (B) ribbon model of aconitase. The different amino acids are labelled as shown. The purple dotted line represents hydrogen bonding. Shown is sialic acid docked onto aspargine 612.

Table 1. List of sialylated N-glycopeptides identified in non-capacitated and capacitated mouse sperm and their regulation during the process of capacitation.

Protein ID	Peptide sequence	Mascot score	Fold change	*p* Value	MS/MS (suppl 1)
Angiotensin-converting enzyme	K.EADNFFTSLGLLPVPPEFW**NK.S**	42.9	ND	ND	1
	K.LITGQP**NMS**ASAMMNYFKPLTEWLVTENR.R *	40.7	ND	ND	2
	K.STEVS**NHT**LK.Y	54.0	-1.09	0.063	3
	K.TFDVSNFQ**NSS**IK.R	76.9	-1.34	0.074	4
Aconitate hydratase, mitochondrial precursor	R.GHLD**NIS**NNLLIGAINIENGK.A *	67.8	2.04	0.016	5
Acrosin precursor	R.VDLIDLDLC**NST**QWYNGR.V	128.0	-1.15	0.113	6

ADAM 26A	R.KEKNECDLPEWC**NGT**SAECPGDVYK.A	80.8	-1.32	0.243	7
ADAM 24	K.LS**NCS**YEVLWAHMI**NK.S**	49.5	ND	ND	8
ADAM 2 precursor	R.AFS**NCS**MEDFSK.F	85.7	ND	ND	9
	R.**NTT**DYVGATYQGK.M	56.0	ND	ND	10
ADAM 5	K.A**NLS**VAYAQIR.D	80.8	1.09	0.314	11
ADAM 1b	K.EGDVCRPADGPCDLEEYC**NGT**SAACPSDR.K	82.6	-1.52	0.081	12
Anthrax toxin receptor-like	K.DFYQV**NIS**GHGL**NNT**SNMK.Q *	62.2	1.53	0.162	13
Beta-2-glycoprotein 1 precursor	K.DYRPSAG**NNS**LYQDTVVFK.C	59.2	1.12	0.264	14
	K.**NIS**FACNPGFFL**NGT**SSSK.C *	116.5	2.06	0.163	15
Sodium/potassium-transporting ATPase subunit beta-3	K.EE**NAT**IATYPEFGVLDLK.Y	85.2	-1.27	0.162	16
Basigin precursor	K.SQLTISNLDVNVDPGTYVC**NAT**NAQGTTR.E *	63.4	1.19	0.063	17
	K.TSDTGEEEAIT**NST**EANGK.Y	151.1	-1.35	0.090	18
Bactericidal permeability-increasing protein	K.T**NAS**LEVDAEENR.L	92.0	-1.27	0.214	19
C4b-binding protein	K.ALCQKPEVG**NGT**LSDEK.D	52.8	-1.30	0.233	20
	R.CEQEASEDLKPALTG**NK.T**	43.1	ND	ND	21
	R.LACL**NGT**VLR.G	76.8	-3.62	0.009	22
Carbonic anhydrase 4 precursor	R.Y**NGS**LTTPNCDETVIWTVYK.Q	88.6	1.71	0.088	23
Carboxypeptidase A5 precursor	K.AGFGG**NGS**NKNPCSETYR.G *	40.3	ND	ND	24
Carboxypeptidase Q	K.EVMNLLQPL**NVT**K.V	80.1	1.43	0.266	25

CD109 antigen homolog precursor	R.FLVTAPGIIRPGA**NVT**IGVDLLEN SPPQVLVK.A *	51.9	-2.03	0.084	26
CD151 antigen	K.LQQEFHCCGS**NNS**QDWQDSEWI R.S	85.7	-1.03	0.466	27
CD59B glycoprotein	K.I**NTT**CSPNLDSCLYAVAGR.Q	89.4	1.02	0.466	28
Clusterin precursor	K.AFPEVC**NET**MMALWEECKPCLK .H *	46.9	-2.55	0.164	29
	R.QEL**NDS**LQVAER.L	72.9	ND	ND	30
Choline transporter-like protein 5	R.CIPDLSAL**NGT**WTPGSR.M	84.3	1.11	0.312	31
Cation channel sperm-associated protein subunit gamma 2	K.LY**NMS**GDYGIPDLFFLDK.G	63.9	-1.30	0.163	32
	R.GVD**NST**YCDYK.L	73.8	ND	ND	33
Cation channel sperm-associated protein subunit beta	K.TPVYNPLGL**NLT**IQGSELFHFK.V *	66.5	ND	ND	34
CUB and zona pellucida-like domain-containing protein 1 precursor	K.ALVLQLSANE**NCT**WTIERPE**NR.S** *	122.2	-1.72	0.181	35
	K.GFSASYTSIYIHDV**NTT**SLSCVSD K.M	89.8	1.77	0.146	36
Dickkopf-like protein 1 precursor	K.VTD**NQT**GEVLISEK.V	79.2	1.04	0.460	37
Dipeptidase 3 precursor	R.HHFYT**NIS**GLTSFGEK.V	101.5	-1.30	0.122	38
	R.MCSAYPELELVTSADGL**NNT**QK. L	150.4	-1.08	0.434	39
Embigin precursor	K.KDDEPLETTGDF**NTT**K.M	75.9	1.42	0.338	40
	K.YII**NGS**HA**NET**R.L	68.4	ND	ND	41
Endoplasmin precursor	K.HN**NDT**QHIWESDSNEFSVIADPR. G *	93.0	-3.89	0.200	42

	R.TDDEVVQREEEAIQLDGL**NAS**QIR.E	85.2	ND	ND	43
Equatorin	K.AV**NET**AVSMDDK.D	96.8	-1.29	0.145	44
	K.DQFFQPIPASDL**NAT**NEDK.L	101.8	1.23	0.241	45
Carboxylesterase 5A	K.HDLQVVANVCDC**NVS**DSK.A	103.1	-1.43	0.323	46
Interferon-induced guanylate-binding protein 1	K.LQEQERLLKQGFQ**NES**LQLR.Q	42.0	-1.22	0.201	47
Glycerophosphodiester phosphodiesterase domain-containing protein 4	K.EVLPSAAG**NHT**SNF**NWT**FLSTLNAGK.W *	91.7	-1.02	0.469	48
Gamma-glutamyltranspeptidase 1 precursor	R.LA**NTT**MF**NNS**K.D	56.2	ND	ND	49
Gamma-glutamyltransferase 7	R.TA**NHS**APSLENSVQPGK.R	49.2	ND	ND	50
Beta-galactosidase-1-like protein	R.CGSLQGLYTTIDFGPAD**NVT**R.I *	45.6	ND	ND	51
Solute carrier family 2, facilitated glucose transporter member 3	K.DFL**NYT**LEER.L	69.6	-1.10	0.271	52
Hexokinase-1	K.SQ**NVS**MESEVYDTPENIVHGSGSQLFDHVAECLGDFMEK.R *	94.2	ND	ND	53
Hyaluronidase PH-20 precursor	K.VG**NAS**DPVPIFVYIR.L	60.6	-1.53	0.102	54
Hypoxia up-regulated protein 1	R.AEPPL**NAS**AGDQEEK.V	61.0	-4.07	0.165	55
	R.VFGSQ**NLT**TVK.L	76.2	ND	ND	56
Izumo sperm-egg fusion protein 1 precursor	R.VWE**NSS**ETLIAK.G	85.7	-1.24	0.129	57
Casein kinase I isoform gamma-2	K.NQAL**NST**NGELNTDDPTAGHSNAPIAAPAEVEVADETK.C *	92.2	-1.32	0.210	58
Laminin subunit alpha-1 precursor	K.LDELK**NLT**SQFQESVD**NIT**K.Q *	50.0	ND	ND	59

Lysosome-associated membrane glycoprotein 1 precursor	R.AF**NIS**P**NDT**SSGSCGINLVTLK.V *	61.4	-3.42	0.113	60
	R.L**NMT**LPDALVPTFSIS**NHS**LK.A *	65.8	ND	ND	61
Epididymal-specific lipocalin-8 precursor	K.AVY**NSS**GSCVTESSLGSER.D	109.7	-1.41	0.162	62
Endothelial lipase	K.DPEQEGC**NLS**LGDSK.L *	79.3	ND	ND	63
	K.IEL**NAT**NTFLVYTEEDLGDLLK.M	71.2	ND	ND	64
	K.LLENCGF**NMT**AK.T	62.7	-1.33	0.011	65
Lipid phosphate phosphohydrolase 1	K.I**NCS**DGYIEDYICQGNEEK.V	120.3	1.06	0.359	66
Leucine-rich repeat-containing protein 52 precursor	K.YVFA**NTT**SLR.Y	52.5	ND	ND	67
	R.L**NIS**HNPHLLYLDK.Y	40.6	ND	ND	68
Ly6/PLAUR domain-containing protein 4 precursor	K.FQAGNL**NTT**FLIMGCAR.D	118.3	1.14	0.299	69
	R.SYLCN**NLT**NLEPFVR.L *	76.6	-1.19	0.270	70
Lysosomal alpha-mannosidase	R.DDYRPTWTL**NQT**EPVAGNYYPV NTR.I *	49.0	ND	ND	71
Epididymis-specific alpha-mannosidase precursor	K.QFF**NAS**VQFDNMDPLLDYINQR. T *	57.0	-2.59	0.155	72
	K.Y**NLT**L**NDT**SIVHPVLWLMLGPK. S	89.7	1.23	0.243	73
Membrane cofactor protein precursor	K.**NGT**HTLTDINVFK.Y	54.3	1.05	0.384	74
Mitochondria-eating protein	R.DNSPDQDQHQSD**NES**FSETQPTQ VQDDLAESGK.S *	61.5	-1.69	0.127	75
Membrane metallo-endopeptidase-like 1	K.NGNMLDWWS**NFS**AR.H	63.0	-1.91	0.118	76
	R.EEMAEVLELETHLA**NAT**VPQEK. R	56.9	-1.24	0.362	77

	R.VLIDLFIWNDDQ**NSS**R.H	58.9	ND	ND	78
Ecto-ADP-ribosyltransferase 3	R.KGTSNDLVLQSI**NST**CSYYECAFLGGLK.T *	86.0	-1.18	0.320	79
	R.LG**NFT**LAYSAKPETADNQR.V *	112.9	1.19	0.079	80
Nicastrin	K.DLYEYSWVQGPWNS**NR.T** *	45.9	ND	ND	81
L-amino-acid oxidase precursor	K.VVTLGL**NR.T**	55.6	-1.34	0.138	82
	R.TLGL**NLT**QFTQYDENTWTEVHNVK.L	97.3	-1.10	0.418	83
Nuclear pore membrane glycoprotein 210-like precursor	K.CFP**NSS**VIEEDGGGLLR.S	99.7	-1.16	0.352	84
	K.EYFEEQLSTS**NGS**YHVVK.A	44.4	-1.90	0.069	85
	K.SS**NET**LAHFEDSK.S	83.2	-1.38	0.051	86
	R.EVVV**NAS**SR.L	58.7	1.01	0.470	87
	R.G**NST**ILAR.D	68.4	-1.78	0.179	88
	R.ILIPFIPGFYM**NQS**EFVLGHK.D	45.3	-1.05	0.467	89
	R.KFD**NFS**SLMLEWK.S	66.6	-1.10	0.315	90
Lysosomal Pro-X carboxypeptidase precursor	K.**NIS**SHSNIIFSNGELDPWSGGGVTR.D *	91.7	ND	ND	91
Protein disulfide-isomerase-like protein of the testis	K.ALLF**NNS**DEVADFVK.S	82.0	-2.69	0.235	92
Phospholipase B1, membrane-associated	K.AE**NLT**SQVR.T	73.6	1.11	0.268	93
	K.NSNLG**NGT**WMVCEER.A	89.7	-1.67	0.053	94
	K.TLE**NVT**TLPNILR.K	42.1	1.00	0.499	95
	R.D**NFT**VVVQPLFE**NVS**MPR.T *	58.5	ND	ND	96
	R.HSQ**NLT**AMQELK.K	78.2	-1.38	0.153	97
	R.DQG**NVT**DMASMK.Y	89.4	-1.10	0.326	98

Putative phospholipase B-like 1	R.F**NET**LHR.G	49.8	-1.23	0.200	99
Prominin-1 precursor	K.DALQ**NMS**SSLK.S	50.1	ND	ND	100
	K.SLQDAATQLNT**NLS**SVR.N	121.1	-1.46	0.244	101
Inactive serine protease 39	R.ILLGYNQLSNPS**NYS**R.Q	104.5	-2.00	0.001	102
Serine protease 42	K.LQHPV**NFT**TNIYPVCIPSESFPVK.A *	84.1	1.22	0.217	103
Serine protease 44	K.GGDACQGDSGGPLVCEF**NK.T**	97.1	-1.61	0.067	104
Serine protease 46	K.VGVQTLPD**NST**SELLVTR.I	100.3	1.15	0.349	105
Serine protease 52	R.NCWVTGWGIT**NTS**EK.G	101.7	-3.09	0.003	106
Prostaglandin-H2 D-isomerase precursor	K.TVVAPSTEGGL**NLT**STFLR.K	141.6	-1.42	0.279	107
Patched domain-containing protein 3	K.VVQE**NGT**QILYQEVCAK.Y	94.7	1.14	0.192	108
	R.FVQGHFST**NDT**YR.F	60.9	-1.17	0.324	109
Pituitary tumor-transforming gene 1 protein-interacting protein precursor	R.VGCSEYT**NR.S**	59.5	-1.02	0.432	110
RING finger protein 126	R.NTE**NGS**APSTAPTDQNR.Q	75.4	ND	ND	111
Solute carrier family 13 member 5	R.AMFNLDNFPDWA**NST**SVNT.-	100.3	1.03	0.472	112
Solute carrier family 22 member 21	R.IPDTV**NLS**SAWR.N	91.2	-1.09	0.201	113
	R.LATIA**NFS**ELGLEPGR.D	96.2	-1.11	0.282	114
Sperm acrosome membrane-associated protein 1 precursor	K.LLKPDQQPVILT**NDS**AVLEITR.E	138.6	1.38	0.258	115
Saccharopine dehydrogenase-like oxidoreductase	K.ACIE**NGT**SCIDICGEPQFLELMHAK.Y	81.0	ND	ND	116
	R.NQM**NGT**LTAVESFLTINTGPEGLCIHDGTWK.S *	91.5	ND	ND	117

Sortilin precursor	R.HLYTTTGGETDFT**NVT**SLR.G	62.3	-2.18	0.053	118
Kunitz-type protease inhibitor 4	R.FFY**NQT**AK.Q	42.0	-1.09	0.317	119
Signal peptide peptidase-like 2B	K.SGNSIMVEVATGPS**NSS**THEK.L	87.6	1.18	0.290	120
Suppressor of G2 allele of SKP1 homolog	R.CQEIQ**NGS**ESEVSASQR.T	84.2	ND	ND	121
Synaptophysin-like protein 1	K.**NQT**VTATFGYPFR.L	89.3	-1.29	0.154	122
Testisin precursor	K.LSSPVTYNNFIQPICLL**NST**YK.F	94.7	-1.35	0.194	123
Testis-expressed sequence 29 protein	K.FAVCDIPLYDICDY**NVT**R.E	101.0	1.02	0.448	124
Transmembrane protease serine 12	R.EEG**NGT**TILQEAK.V	43.0	ND	ND	125
Testis-expressed protein 101 precursor	R.HCPTCVALGSCSSAPSMPCA**NGT**TQCYQGR.L	75.2	-1.99	0.004	126
	R.TF**NWT**SK.A	48.7	-1.91	0.001	127
	R.VPETTATS**NMS**GTR.H	93.3	-2.01	0.001	128
Ubiquitin carboxyl-terminal hydrolase 7	R.ITQNPVING**NVT**LSDGHSNAEED MEDDTSWR.S *	109.5	ND	ND	129
Zonadhesin precursor	K.CPLGTECKDSVDGGS**NCT**K.I	51.9	ND	ND	130
	K.DAQGDLIPA**NK.T**	74.4	-1.24	0.189	131
	K.DGSS**NCT**NIPLQCPAHSR.Y	93.0	-1.14	0.183	132
	K.FQCPSETYCKDIEDGNS**NCT**R.I	43.0	ND	ND	133
	K.TCTTLCTCSAHS**NIT**CSPTACK.A	52.2	-1.04	0.236	134
	R.VGSQSSGWM**NSS**VTIPK.G	52.6	-2.06	0.009	135
Zona pellucida sperm-binding protein 3 receptor precursor	K.GVCLKPMVING**NLS**VER.V	63.8	1.58	0.191	136
	K.TYLFGHEE**NST**EHAMK.G	63.8	-1.64	0.137	137

	R.ASLNDPQTVTCQE**NLT**WSSTNGCER.I	137.3	-1.03	0.357	138
	R.LALFTFP**NIS**ET**NVTNK.T** *	95.9	1.27	0.191	139
	R.V**NSS**HLSCDE**NGS**WVYSTFCAR.K *	75.1	1.08	0.281	140
Zona pellucida-binding protein 1 precursor	R.DGTHCLQC**NNS**LVYGAK.T *	104.7	1.02	0.435	141
Zona pellucida-binding protein 2	K.GNSQI**NIT**NTGELVLK.D *	76.5	1.70	0.145	142

787

788 * ambiguous localization of deamidated residue.

789 Consensus sequence for N-glycosylation is shown underlined and in boldface.

790 Numbers in MS/MS column correspond to page in supplementary I which contains MS/MS
791 spectrum of the glycopeptides.

792 ND (not determined) is used when the area under the curve could not be measured in all samples.

Fig. 1

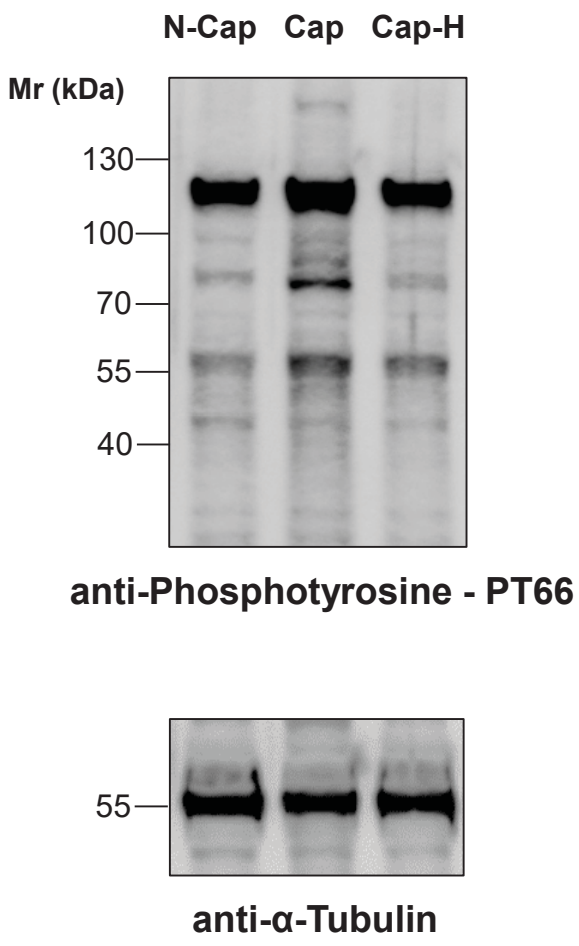

Fig. 2

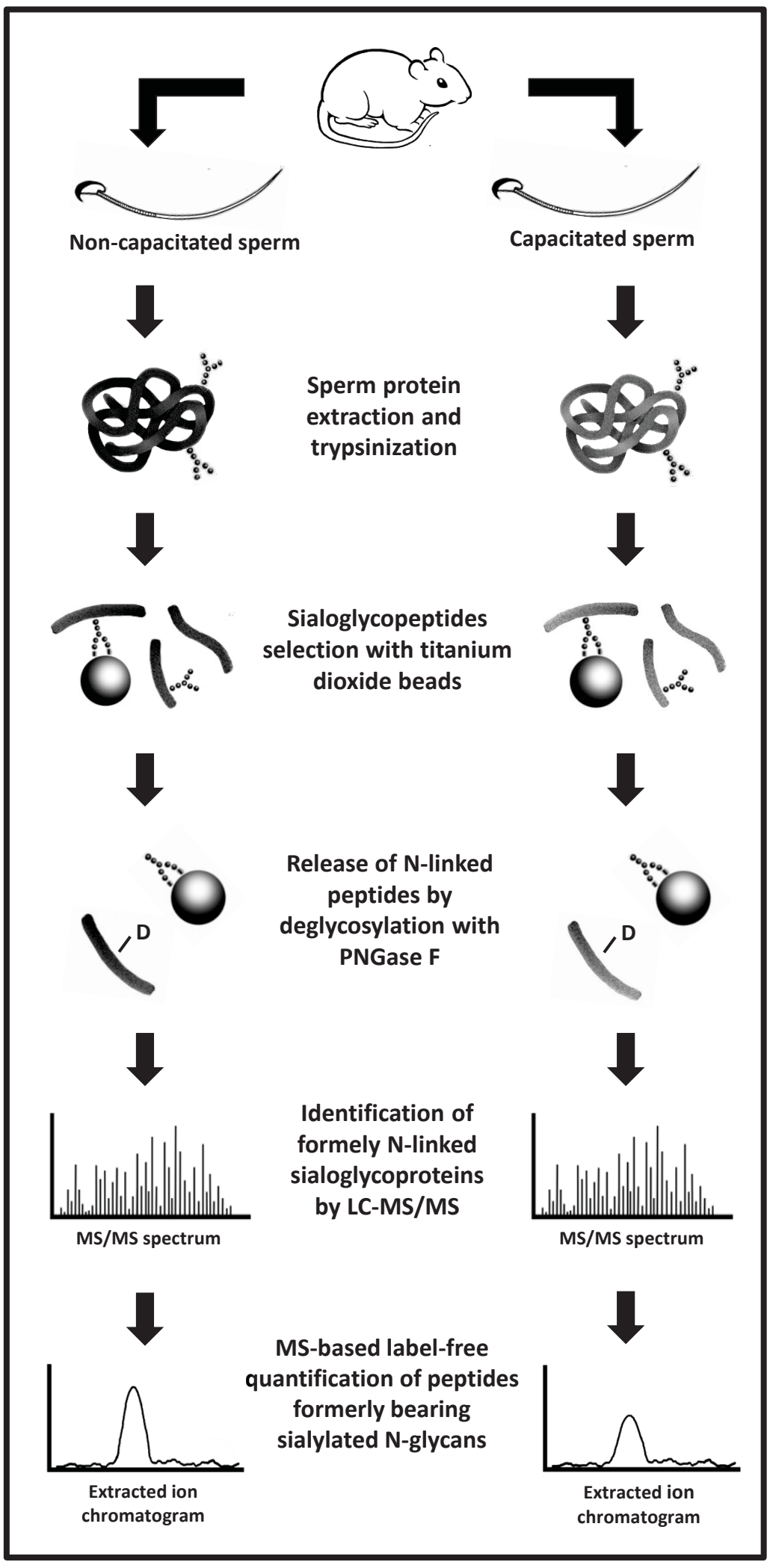

Fig. 3

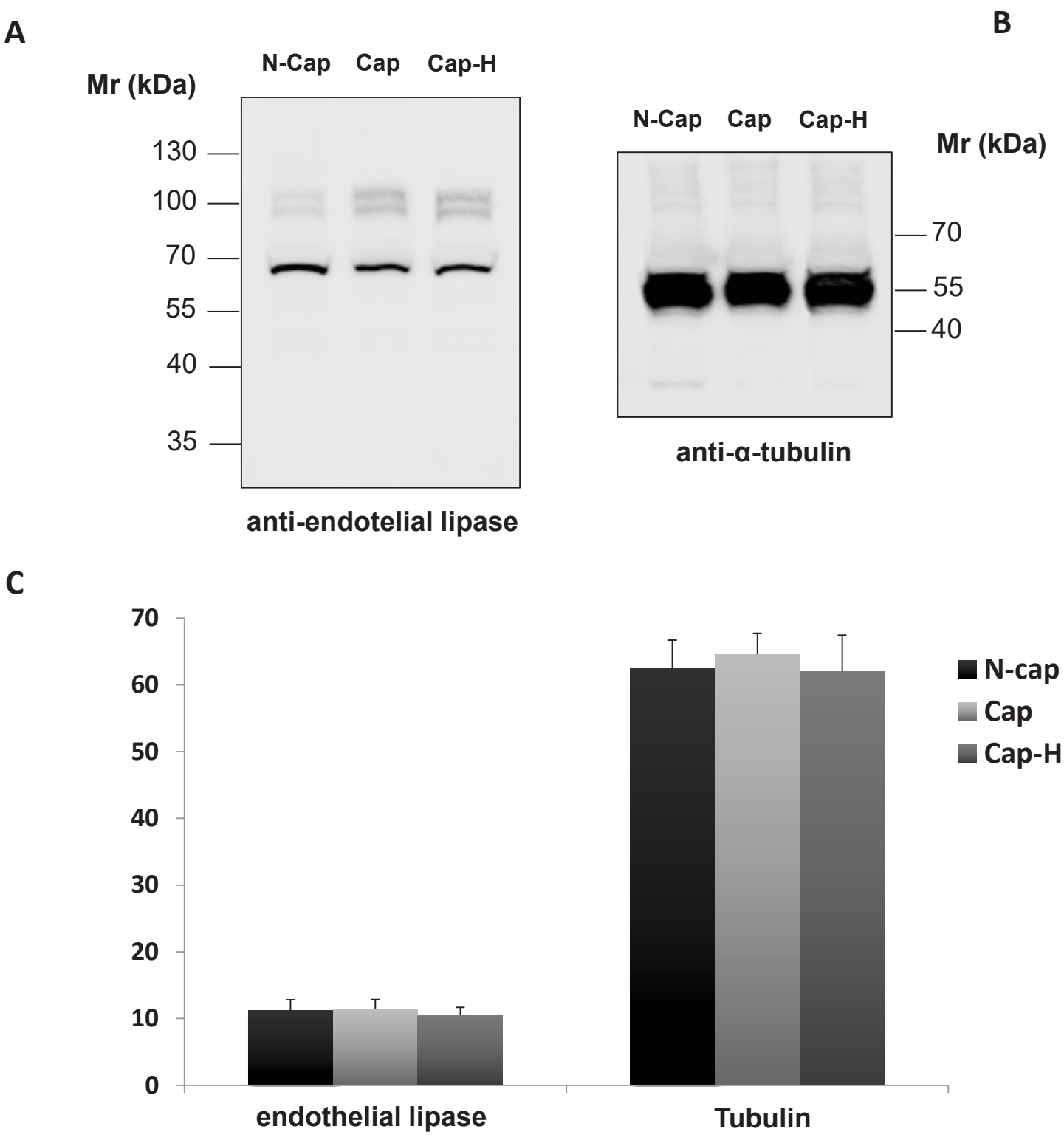

Noncapacitated

Capacitated

Fig. 4

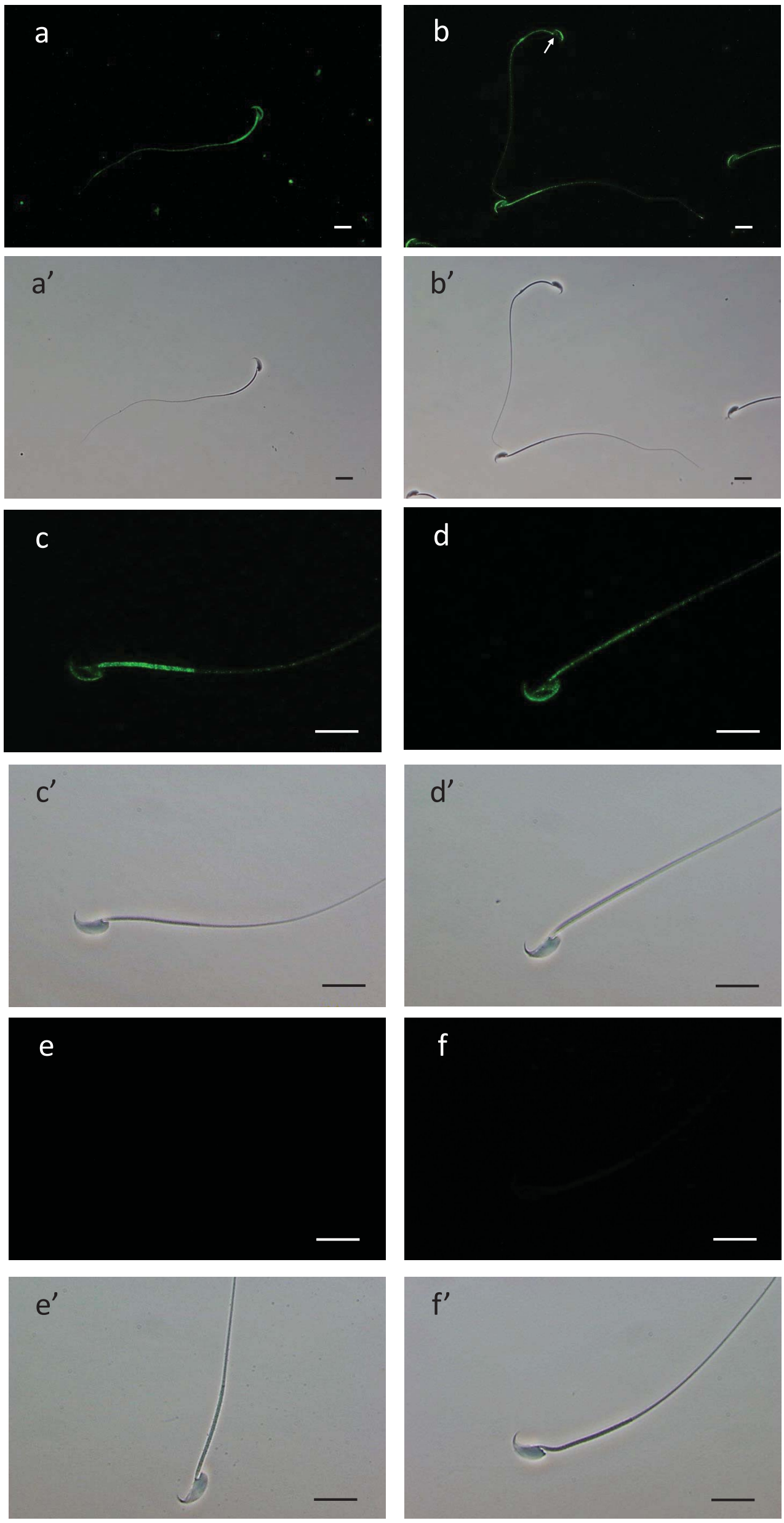

Fig. 5

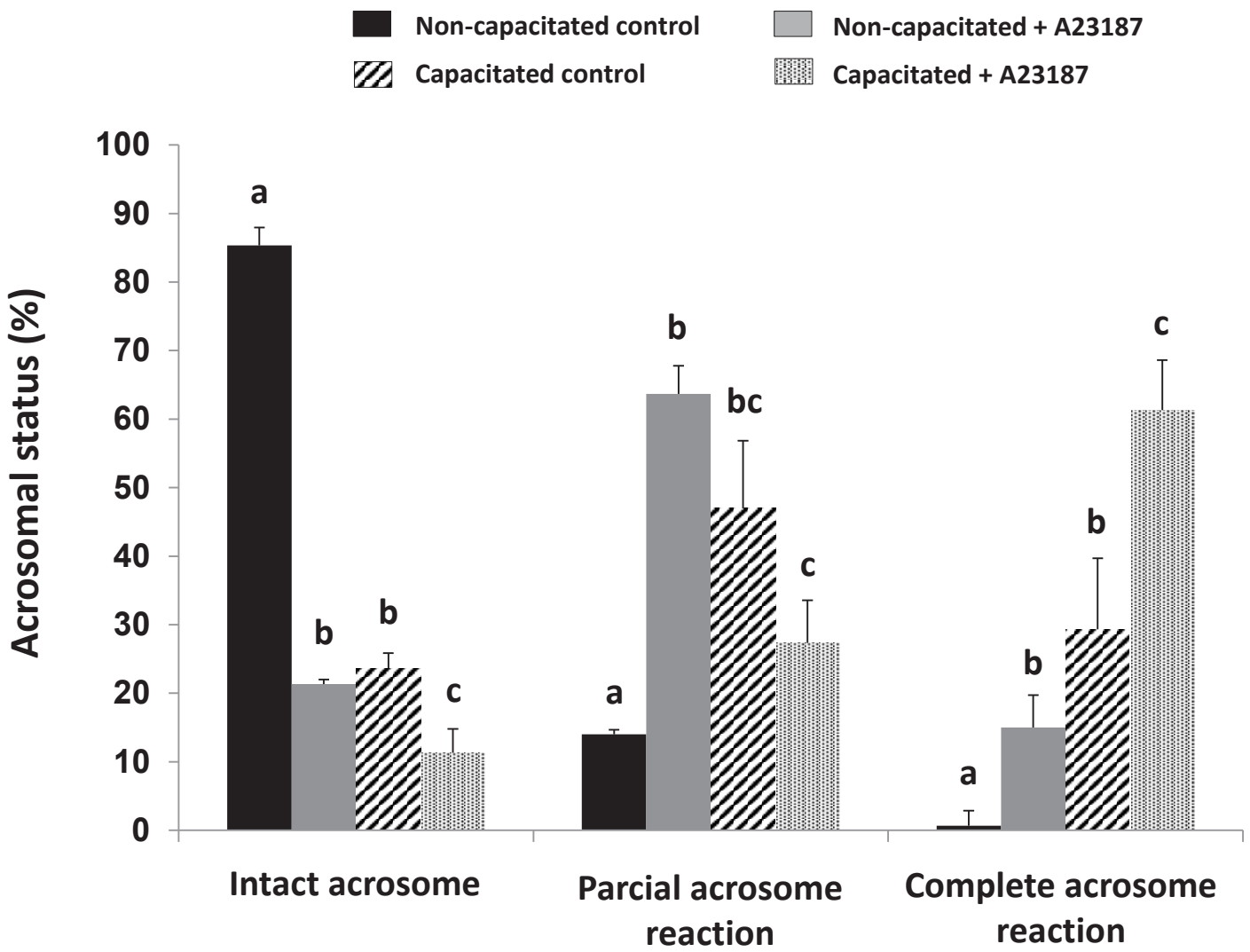

Fig. 6

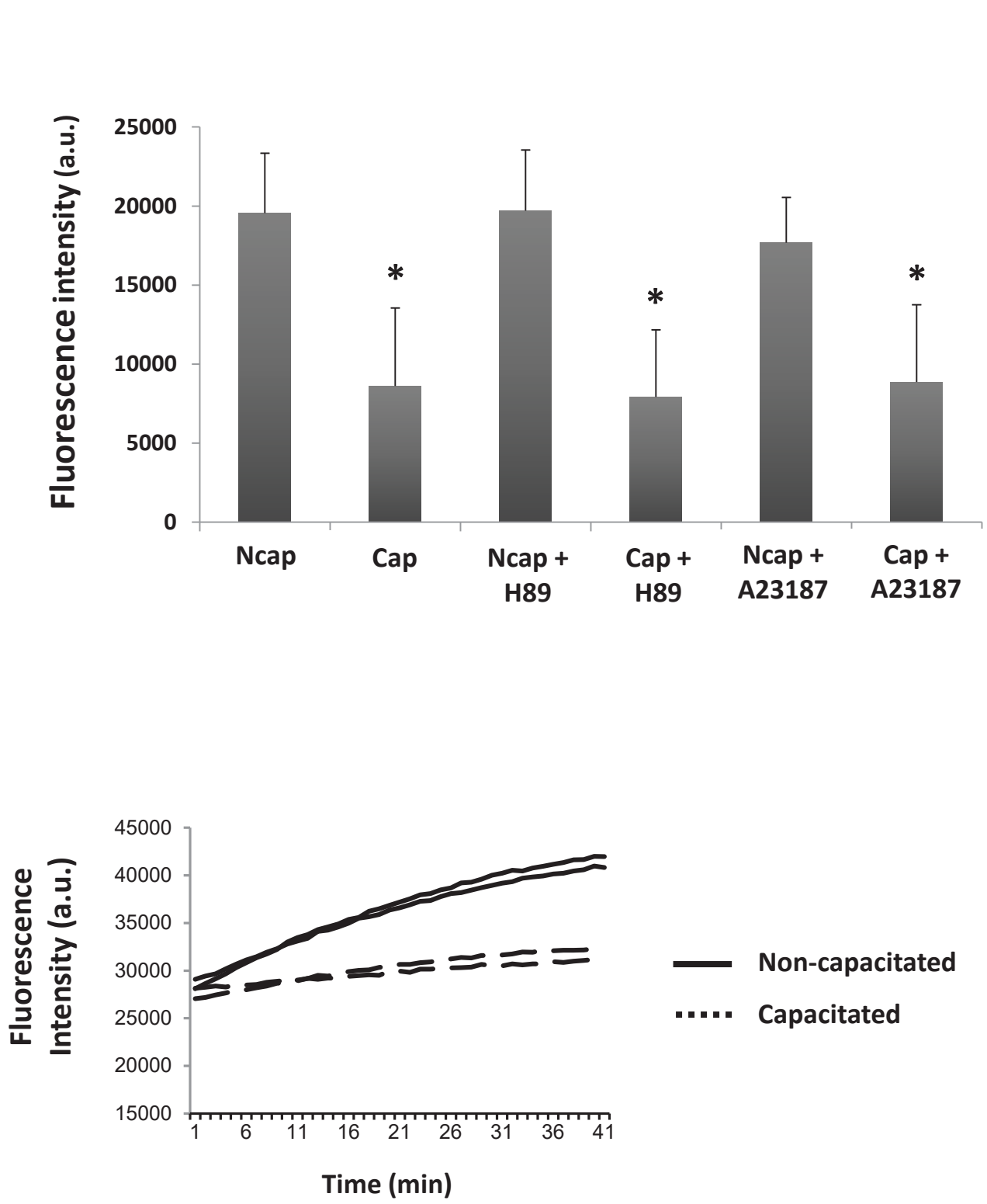

Fig. 7

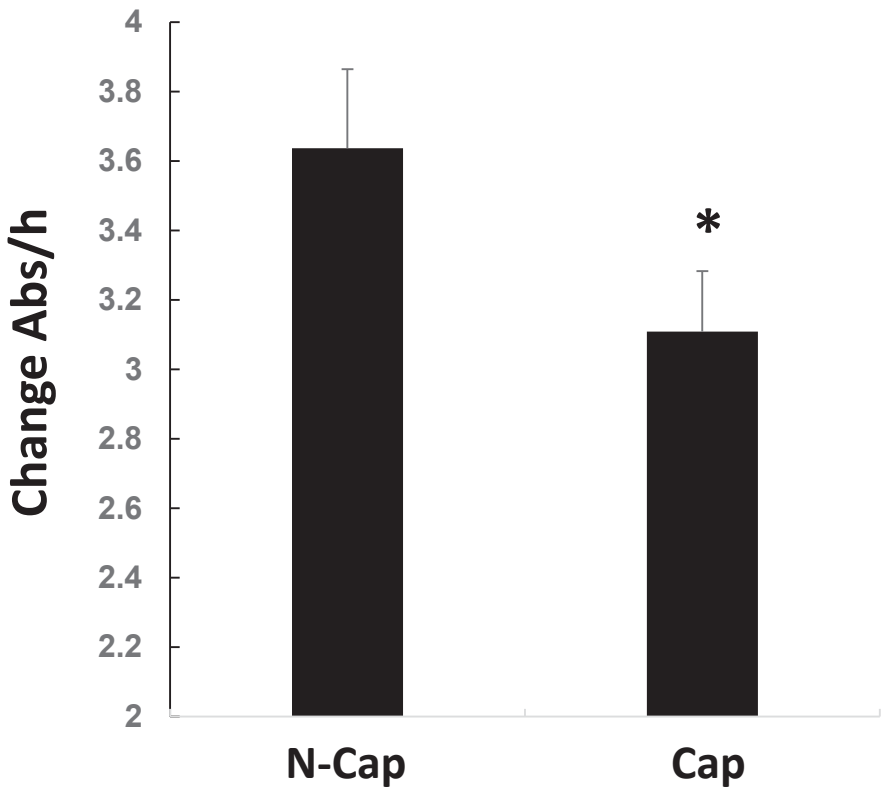

Fig. 8

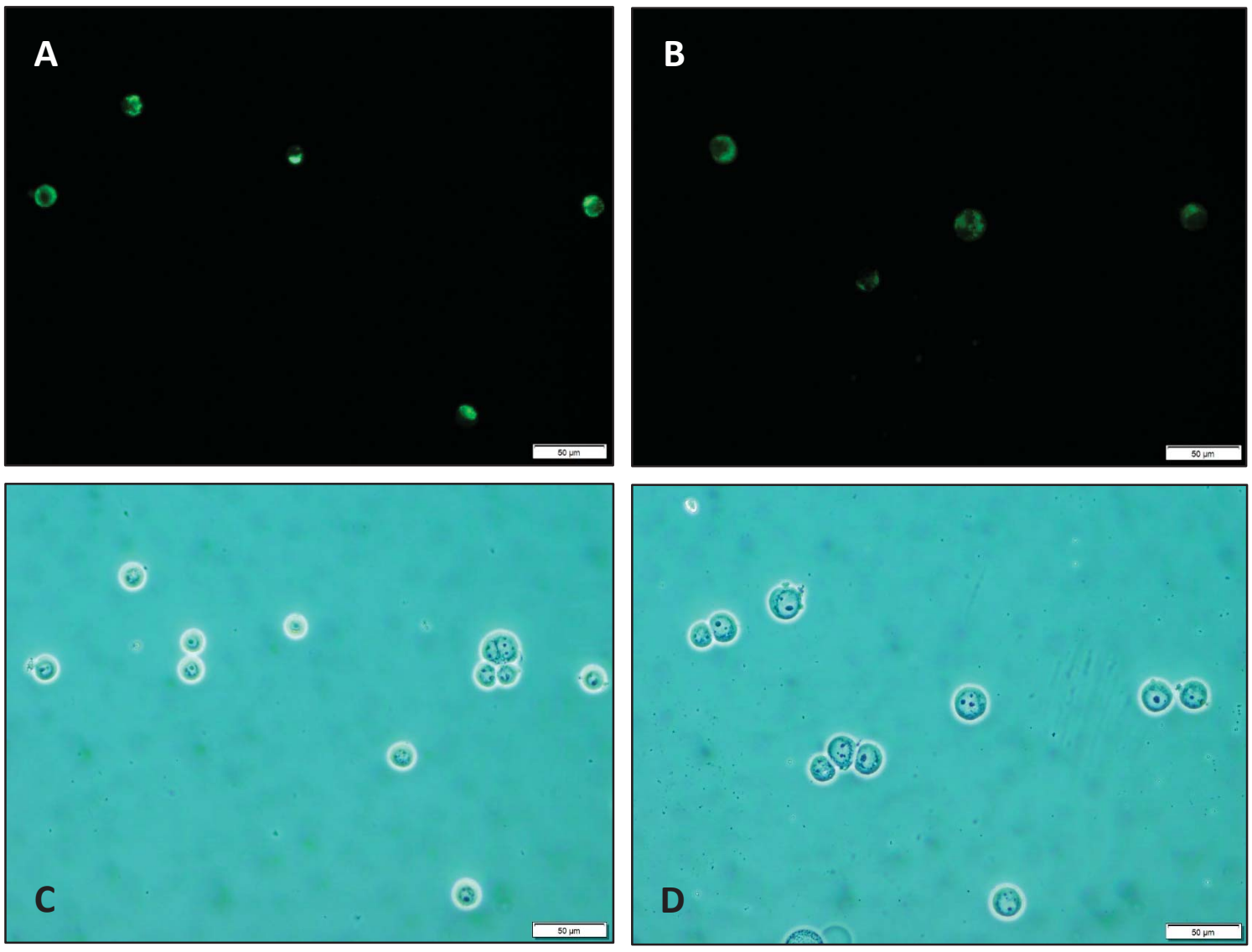

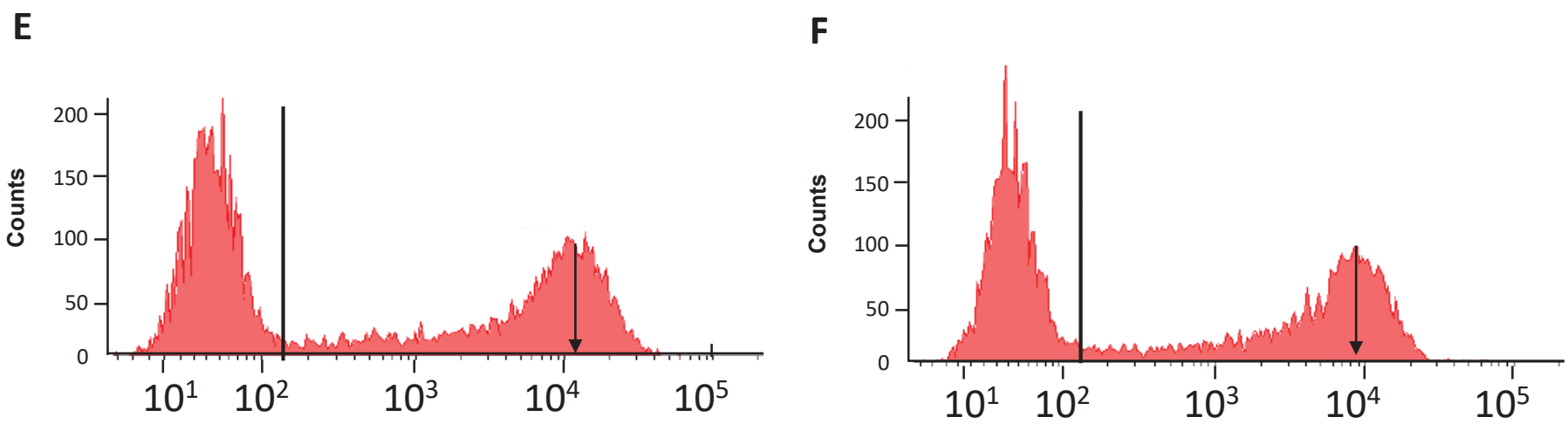

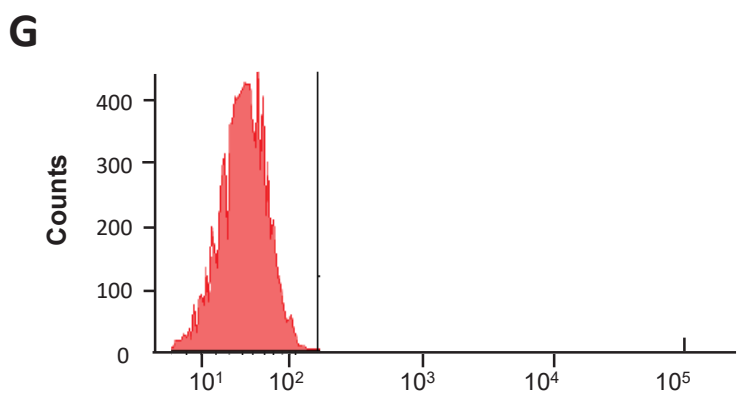

Fig. 9

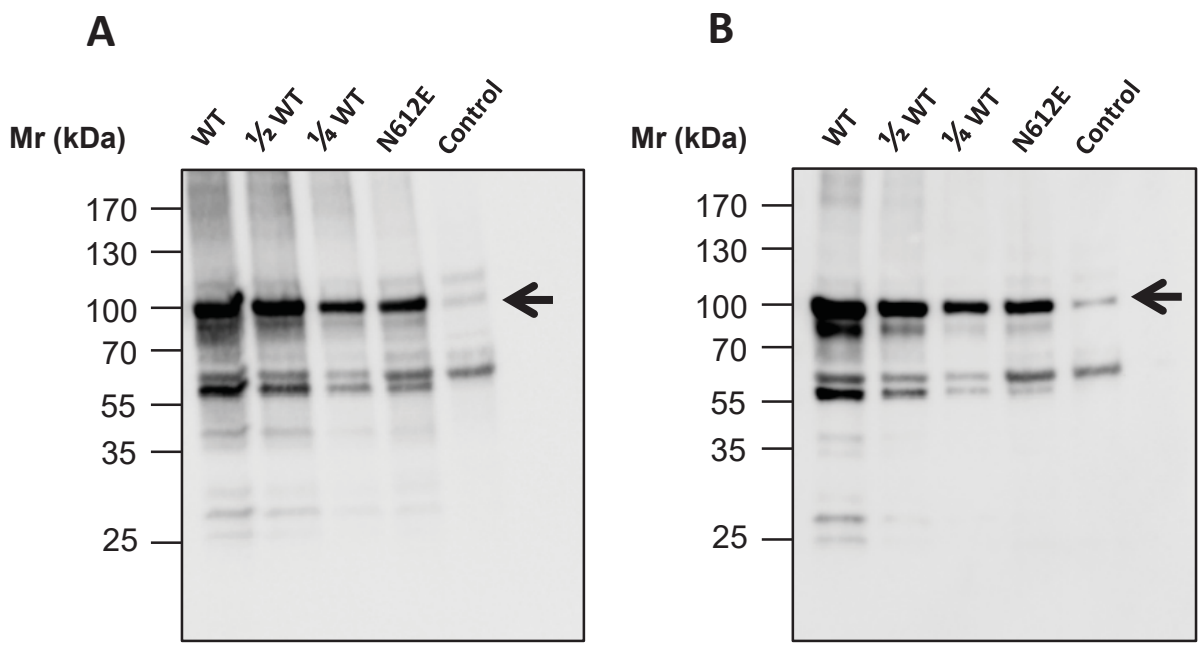

Fig. 10

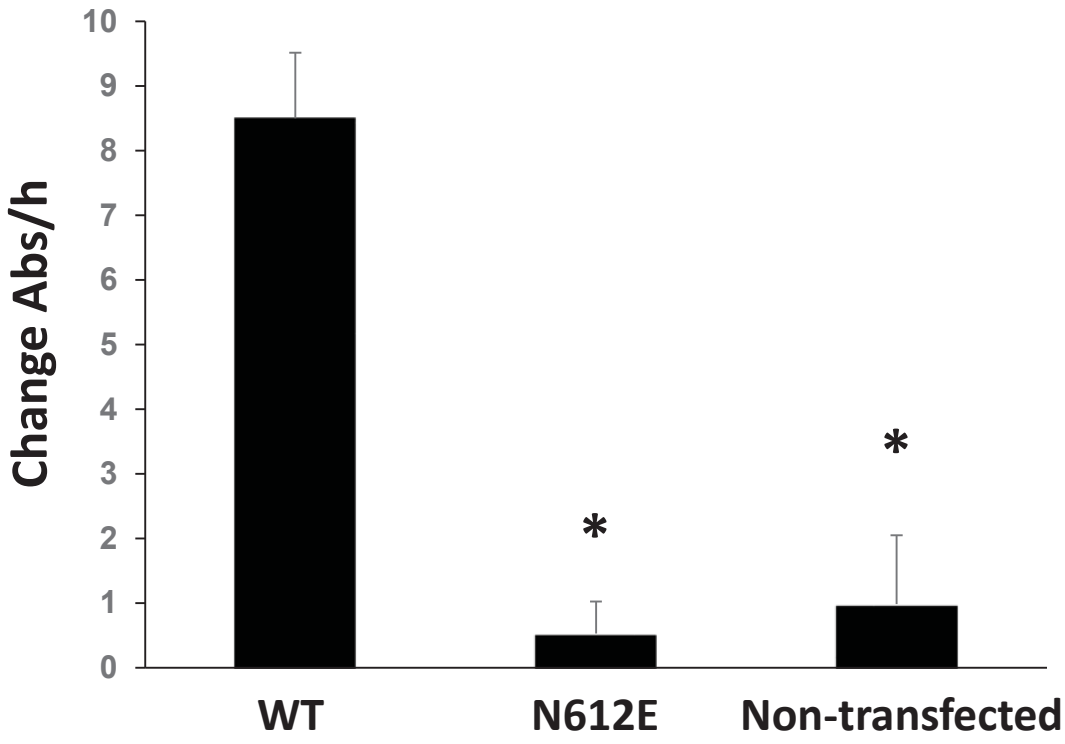

Fig. 11

A)

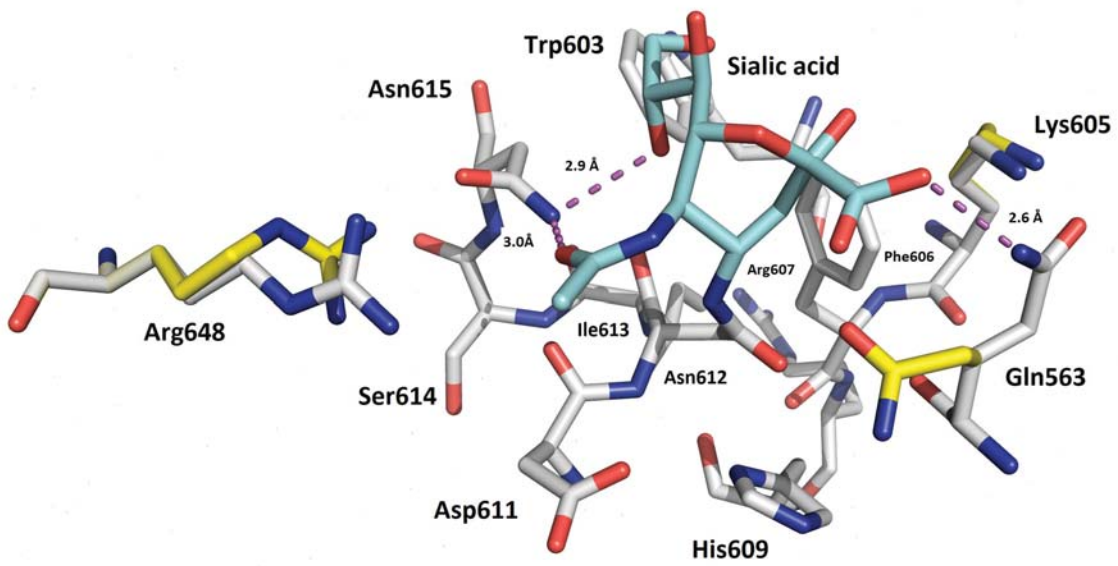

B)